B3-2

Logged in 5/15/85
Kung

CONTRACTOR REPORT

SAND84—7202
Unlimited Release
UC—70

Hydrologic Mechanisms Governing Fluid Flow in Partially Saturated, Fractured, Porous Tuff at Yucca Mountain

J. S. Y. Wang, T. N. Narasimhan
Earth Sciences Division
Lawrence Berkeley Laboratory
University of California
Berkeley, CA 94720

Prepared by Sandia National Laboratories Albuquerque, New Mexico 87185 and Livermore, California 94550 for the United States Department of Energy under Contract DE-AC04-76DP00789

Printed April 1985

Issued by Sandia National Laboratories, operated for the United States Department of Energy by Sandia Corporation.

Printed in the United States of America
Available from
National Technical Information Service
U.S. Department of Commerce
5285 Port Royal Road
Springfield, VA 22161

NTIS price codes
Printed copy: A04
Microfiche copy: A01

Distribution
Category UC-70

SAND84-7202
LBL-18473

Unlimited Release
Printed April 1985

HYDROLOGIC MECHANISMS GOVERNING FLUID FLOW IN PARTIALLY SATURATED, FRACTURED, POROUS TUFF AT YUCCA MOUNTAIN

by

J. S. Y. Wang and T. N. Narasimhan
Earth Sciences Division
Lawrence Berkeley Laboratory
University of California
Berkeley, California 94720

for

Sandia National Laboratories
P.O. Box 5800
Albuquerque, New Mexico 87185

Under Sandia Contract 47-7550

Sandia Contract Monitor

Scott Sinnock
Geoscience Analysis Division

ABSTRACT

An understanding of the mechanisms governing fluid flow in partially saturated, fractured tuff is needed for assessing the suitability of Yucca Mountain in southern Nevada as a potential site for a radioactive waste repository. Fluid flow in partially saturated, fractured tuff is different from the fluid flow in saturated media. In saturated, fractured zones, fluid generally moves along fractures. Because fractures generally have large apertures relative to the size of the matrix pores and the capillary forces are stronger to hold fluid in the smaller pores, fractures in the unsaturated zone would tend to desaturate more easily than the pores in the rock matrix during a drainage process. As a result, the bulk of fluid would move almost entirely through interconnected pores in the matrix. Within partially drained fractures, relatively continuous air phase will produce a practically infinite resistance to liquid flow along the fractures. Flow will be constrained to a direction that crosses, rather than follows, fracture surfaces. The residual liquid in fractures will be held by capillary forces near areas where adjoining fracture surfaces are in contact and apertures are small. The area available for liquid flow from one matrix block to another is restricted to the saturated regions around fracture contact areas. In this report, a general statistical theory is proposed to describe flow along and across fractures that separate partially saturated matrix blocks. This theory incorporates a model for estimating fracture aperture distributions and yields expressions for fracture saturation, fracture permeability, and effective areas of matrix-fracture flow as functions of pressure. With these expressions, drainage of a fractured tuff column was simulated using the TRUST numerical model. The

values for parameters in the expressions are deduced from observations of fracture spacings and orientations in samples from Yucca Mountain, measurements of pressure-saturation relationships of matrix core samples and indirectly derived fracture-surface characteristics. In the simulations of the draining column, discrete vertical and horizontal fractures and intervening matrix blocks were explicitly taken into account. The simulations indicate that the transient change from fully saturated conditions to partially saturated conditions depends strongly on the fracture properties. The simulations also show that changes in fluid flow under nearly steady-state conditions in a partially saturated, fractured, porous system could be simulated approximately without taking the fractures into account.

ACKNOWLEDGEMENTS

We thank S. Sinnock and N. Hayden of Sandia National Laboratories for discussing the tuff data, R. Spengler, R. Scott, and P. Montazer of U. S. Geological Survey for discussing the fracture data. We also thank our collegues Y. Tsang and K. Pruess for discussing and reviewing the manuscript. This work was supported by the Sandia National Laboratories for the Nevada Nuclear Waste Storage Investigation Project of the U.S. Department of Energy.

CONTENTS

FIGURES

FIGURES

GLOSSARY

anisotropic	Having physical properties that vary with direction.
asperity	A type of surface roughness appearing along the fracture surfaces.
bimodal	A distribution with two peaks.
capillary pressure	The difference between the air-phase pressure and the water-phase pressure across a meniscus. If the air-phase pressure is atmospheric, capillary pressure is gauge pressure.
Darcy velocity	Bulk velocity of fluid flow as described by Darcy's law.
fracture plane inclination	The angle from horizontal of the plane of fracture in a rock formation.
isotropic	Having the same properties in all directions.
matrix	The interconnected mass of rock and interstitial pores within which water movement is governed by the laws of porous media flow.
pressure head	Pressure expressed as the height of a column of water that can be supported by the pressure.
tortuosity	A parameter describing the extent to which a fluid-flow departs from a straight path along flow line. Tortuosity results from the diversion of fluid flow around nonconducting volumes in the flow region.

NOMENCLATURE

b	fracture aperture	[L]
b_o	fracture aperture for a fracture under zero stress and with some fracture asperities in point-contact but with zero contact area	[L]
b_c	fracture contact cutoff aperture, portions of fracture with b_o less than b_c will be in contact	[L]
b_s	saturation cutoff aperture, portions of fracture with aperture greater than b_s will be desaturated	[L]
D	fracture spacing	[L]
f	fracture frequency	[1/L]
$f(b)$	aperture distribution functions for a fracture under stress, $f(b) = n(b_o) = n(b + b_c)$	[1/L]
g	gravitational acceleration	[L/t^2]
h	pressure head	[L]
h_c	capillary head	[L]
i	hydraulic gradient	
k	continuum saturated permeability	[L^2]
k_r	relative permeability of liquid flow under partially saturated condition, expressed as a fraction of k	[L^2/L^2]
$n(b_o)$	aperture distribution function for a fracture under zero stress with some fracture asperities in point-contact and with zero contact area	[1/L]
Q	volumetric flow rate	[L^3/t]
S	saturation	[L^3/L^3]
S_r	residual saturation, the amount of water held in the rock	[L^3/L^3]
W	width of the flow path along a fracture	[L]
W_s	width of liquid flow path between dry portions (air pockets) in a fracture	[L]

NOMENCLATURE

β	aperture gamma distribution parameter	[1/L]
γ	surface tension of water	[M/t^2]
ρ	fluid density	[M/L^3]
σ	fraction of surface area saturated with liquid water plus contact areas between adjacent matrix blocks	[L^2/L^2]
θ	angle of contact between liquid surface and solid surface	[radian]
τ	phase separation constriction factor, ratio of width of liquid flow path to the nearest-neighbor dry pocket distance	[L/L]
μ	fluid viscosity	[M/Lt]
ω	fraction of fracture surface area occupied by contact between adjacent matrix blocks	[L^2/L^2]

Subscript

1	saturated condition S = 1
H	horizontal fracture set
S	partially saturated condition at saturation S
V	vertical fracture set
f	fracture
m	rock matrix

INTRODUCTION

The work described in this report was performed for Sandia National Laboratories (SNL) as a part of the Nevada Nuclear Waste Storage Investigations (NNSWI) Project. The NNWSI Project is administered by the U.S. Department of Energy's (DOE) Nevada Operations Office. The project is a part of the DOE's program to safely dispose of the radioactive waste from nuclear power plants. DOE has determined that the safest and most feasible method currently known for the disposal of such wastes is to emplace them in mined geologic repositories. The NNWSI project is evaluating the suitability of Yucca Mountain on and adjacent to the Nevada Test Site (NTS) in southern Nevada to determine the feasibility of developing a repository for high level nuclear wastes.

The objective of this report is to aid the performance assessment activities in the NNWSI Project by addressing the hydrologic mechanisms governing fluid flow in partially saturated, fractured, porous tuff at Yucca Mountain. The focus of this report is on understanding how fractures and porous matrix affect the transient and steady-state fluid flow behavior. The goal is to determine whether a partially saturated, fractured, porous tuff can be idealized as an equivalent continuum combining properties of the fractures and matrix, or as a system of multiple continua in which the fractures, matrix, and their interactions are modeled.

One of the candidate rock units for a nuclear waste repository at Yucca Mountain is the densely welded, devitrified, nonlithophysal zone of tne Topopah Spring Member of the Paintbrush Tuff above the water table. This unit

occurs extensively in the area being considered for a potential repository. Densely welded ash-flow tuffs generally have low matrix hydraulic conductivities but tend to contain numerous fractures that may be highly transmissive (Sinnock et al., 1984). Fractures may be important either as conduits or as barriers for flow of groundwater. In the saturated zone, water tends to move rapidly along fractures. However, for a fractured unit above the water table, the fractures (whose apertures are large relative to the size of the pores in the matrix) should be nearly dry, and the bulk of the groundwater movement should be through interconnected pores in the matrix. Under this condition, as water moves from one matrix block to another, the drained portions of the fractures will restrict the effective area for water flow from one matrix block to another matrix block.

In this report, we will (1) describe a conceptual model for the hydrology of a partially saturated, fractured, porous medium; (2) construct a general statistical theory for flow along the fractures and for flow between the matrix blocks and the fractures under partially saturated conditions; (3) present the results obtained from a simple statistical aperture distribution model for fracture saturation, hydraulic conductivity, and effective matrix-fracture flow area as functions of pressure; (4) review the available data for the fractured Topopah Spring Member and the needs for additional data to improve and validate the statistical theory; (5) summarize the recent updates of the numerical code TRUST for handling partially saturated, fractured, porous flow systems; and (6) present the results of simulations of a fractured tuff column in response to drainage.

CONCEPTUAL MODEL

To study the flow of water in a partially saturated fractured porous medium, we first formulate a conceptual model based on the basic principles of soil physics. Tuff is a consolidated rock made up essentially of cemented volcanic ash. The primary pore size of the tuff at Yucca Mountain is assumed to range from a few to a few tens of microns. Even at a depth of several hundred meters in such a formation, the fractures are likely to have apertures ranging from several tens to several hundreds of microns. Thus, fractured tuff will have a strongly bimodal pore-size distribution. It is well established in the field of soil physics that in partially saturated porous media, the fluid pressure in the water phase is less than atmospheric pressure and that the fluid saturation in the porous medium is a strong function of the water-phase pressure. The relation between fluid pressure and saturation is governed by surface tension between the liquid and the solid phases and by the effective capillary radii of the pores. Indeed, it is accepted knowledge that as the water-phase pressure in the porous medium is decreased below atmospheric pressure, the largest pores will desaturate first, followed by the desaturation of successively smaller pores.

If one recognizes that the large pores desaturate first during the drainage process, it is easy to infer that the fractures in a fractured porous medium will tend to remain essentially dry under conditions of partial saturation and that water will be held by capillarity in the finer pores of the matrix. Because natural fractures are characterized by rough surfaces, the aperture of a fracture is seldom spatially constant and will be very small near asperities. Thus, one would expect that asperities will cause

"islands" of water film to be held near the contact points between adjacent matrix blocks within the fracture plane. Within a fracture that is partially saturated in this fashion, the presence of a relatively continuous air phase will produce an almost infinite resistance to liquid flow in a direction parallel to the fracture. Therefore, as a fracture begins to desaturate, its effective hydraulic conductivity will decline abruptly by several to many orders of magnitude. It is reasonable to expect that during fracture desaturation the effective hydraulic conductivity of the fractures will rapidly become smaller than that of the porous matrix, which needs fairly large capillary pressures to initiate desaturation.

An interesting consequence of this dramatic reduction in fracture permeability is that water in partially saturated conditions will tend to flow across fractures from one matrix block to another instead of flowing along the fractures. Thus, one may expect flow lines through the rock mass to circumvent dry portions of the fractures (Figure 1) and the fractures will introduce a macroscopic tortuosity in the system. If this reasoning is sound, one may grossly quantify the effects of the fractures in terms of an overall tortuosity factor, a task that may prove to be somewhat simpler than characterizing a saturated fractured system as an equivalent anisotropic medium.

In order to quantitatively evaluate the hydrology of a fractured porous medium, three basic relations are required: (1) the relation between fluid pressure head (which is less than atmospheric under partial saturation) and fracture saturation, (2) the relation between fluid pressure head and fracture conductivity, and (3) the proportion of the fracture surface that remains wetted. To date, no experimental data are available for these

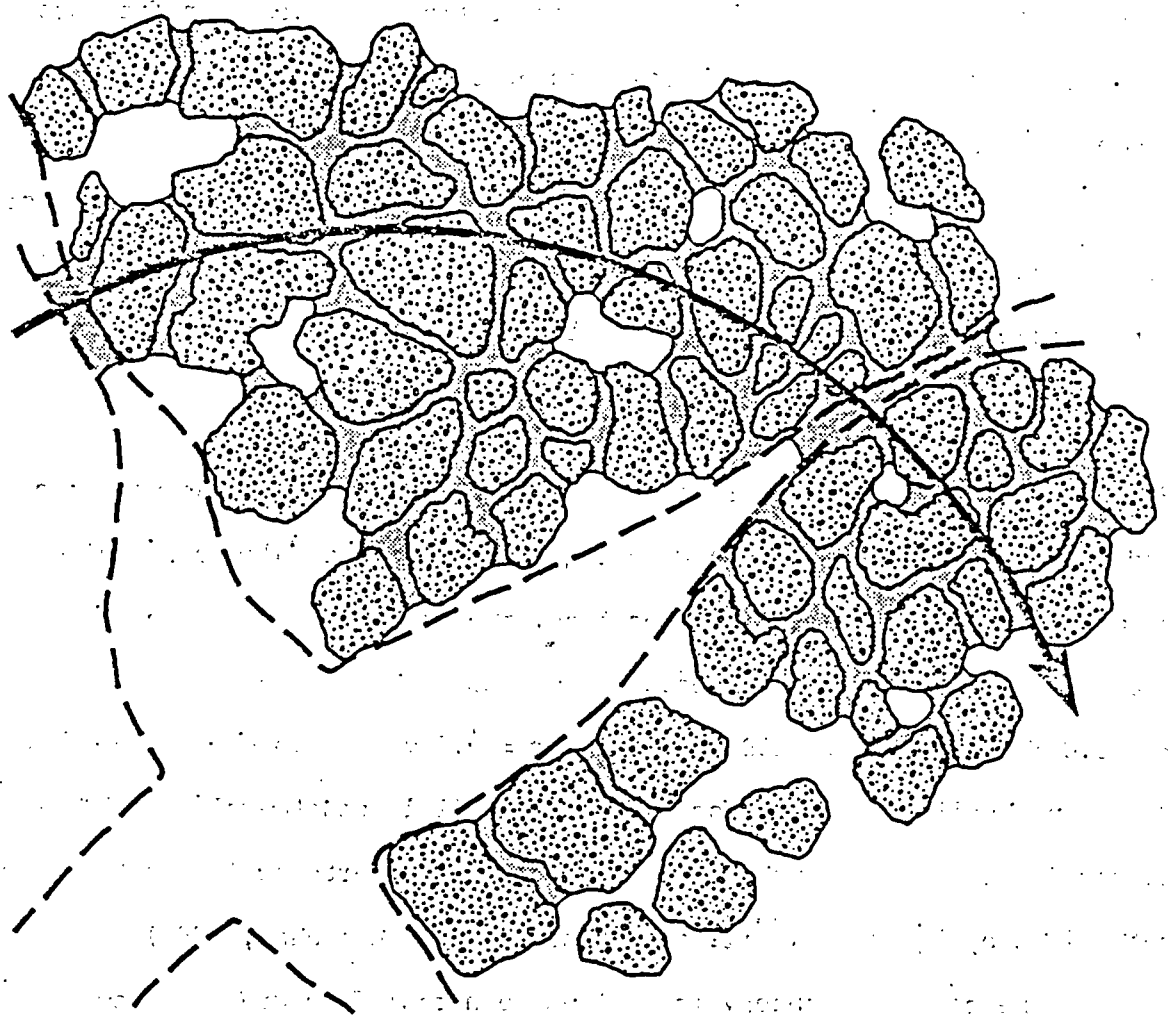

XBL 841-9580

Figure 1. Conceptual model of partially saturated, fractured, porous medium showing schematically the flow lines moving around the dry portions of the fractures.

relations for the Yucca Mountain rocks. In order to gain insight into the problem, it is necessary to develop these relations on theoretical grounds using fracture roughness characteristics and surface tension characteristics. The capillary theory and rough fracture flow law are the building blocks with which we construct our development of theoretical formulae for fracture saturation, hydraulic conductivity, and effective fracture surface area for rough fractures.

Capillary pressure determines the water-phase pressure at which a given size fracture or pore will drain. From force balance, the height of rise for an idealized parallel-plate, smooth-wall fracture with aperture b is

$$h_c = -h = \frac{2\gamma\cos\theta}{b\rho g} \quad . \tag{1}$$

With the gravitational acceleration g, water density ρ, surface tension γ, and the angle of contact θ between liquid surface and solid surface remaining constant at ambient temperature, the capillary head h_c or the pressure head h is inversely proportional to the aperture b. We use $\theta = 0°$, $\gamma = 0.072$ kg/sec^2, $\rho = 1000$ kg/m^3, and $g = 9.8$ m/sec^2 in our calculations. Using the capillary theory for a set of parallel, smooth-wall fractures at given negative pressure head, h, fractures with apertures larger than those determined by Equation 1 will be drained (Evans and Huang, 1982).

If the capillary theory is applied to a real fracture with rough wall and variable aperture, this equation indicates that the sections with large apertures will drain first as the magnitude of the capillary suction increases (or the pressure head becomes more negative). Two important phenomena will occur as the fracture desaturates: (1) along the fracture surface, air

pockets will form and impede the flow, thereby reducing its effective permeability for liquid flow, (2) normal to the fracture surface, the flow between adjacent matrix blocks across the fractures will occur only through the sections of the fracture that remain saturated. Unsaturated portions within the fractures will then become barriers to liquid flow both along the fractures and normal to the fractures between the adjacent matrix blocks.

In this simple model, we ignore film flow on partially saturated rock surfaces, vapor transport from evaporation-condensation across the liquid phases, drying processes of isolated liquid pockets surrounded by gaseous phases, and solubility of air in water. It is possible to extend the quantitative statistical theory to be presented in the next section to include these phenomena. However, for simplicity, we will ignore these mechanisms and focus on the consequences induced by the desaturation of fractures on the liquid fluid flow through partially saturated, fractured, porous tuff.

STATISTICAL THEORY FOR PARTIALLY SATURATED FLOW IN ROUGH FRACTURES

The scale of primary interest in our study is of the order of the size of matrix blocks separated by discrete fractures. The much smaller scale around individual fracture asperities is not of practical interest for fluid-flow modeling. A statistical averaging procedure, applied over this smaller scale, is assumed to be sufficient to take into account the controlling mechanisms governing the desaturation of sections of larger apertures and the resultant reduction in fracture and matrix flows.

The statistical description of a rough-wall, variable-aperture fracture

begins with the aperture distribution function $n(b_o)$ for a fracture under zero stress (Tsang and Witherspoon, 1981). Under zero stress, the fracture surfaces are in point contact with zero contact area between the walls. The aperture distribution function $n(b_o)$ can be measured by scanning the open fracture surfaces and tracing the roughness profiles. The mismatch between the roughness profiles between the two surfaces yields the aperture distribution function $n(b_o)$ (Tsang, 1984).

For in situ fractures, the stress is greater than zero, and finite (non-zero) area of fracture surfaces will be in contact. The fraction of contact area, ω, of the total area of the fracture at any stress can be expressed as

$$\omega = \int_0^{b_c} n(b_o)db_o \quad . \tag{2}$$

The averaging over aperture is equivalent to normalized areal integration over the surface of the fracture plane. All portions of a fracture with initial apertures less than the contact cutoff aperture b_c will be in contact. The apertures under stress will be $b = b_o - b_c$ in the open sections of the fracture. The aperture distribution of a fracture under stress will be denoted by $f(b)$, which is

$$f(b) = n(b + b_c) \quad . \tag{3}$$

For fully saturated flow of water in the fractures, the cubic law, derived from the solution of an idealized parallel plate representation of the fracture (Boussinesq, 1868), is valid from experimental studies on a set of artificially induced tension fractures in hardrock samples (Witherspoon et al., 1980). For laminar flow through a fracture with lateral width W and with uniform aperture b, the volumetric flow rate Q is

$$Q = W \cdot \frac{\rho g}{\mu} \cdot \frac{b^3}{12} \cdot i \quad , \tag{4}$$

where i is the hydraulic gradient and μ is the fluid viscosity. For a fracture with variable aperture, one may generalize the cubic law by replacing the cube of the single value for the aperture by an average $\langle b^3 \rangle$

$$\langle b^3 \rangle_1 = \int_0^{b_{max}} b^3 \, f(b) db \quad . \tag{5}$$

If this generalization of the cubic law is valid, then this average $\langle b^3 \rangle_1$ determines the saturated conductivity of a variable-aperture fracture. The subscript 1 denotes the saturated condition $S = 1$.

The basic assumption in using $\langle b^3 \rangle$ is that all the flow paths within a fracture are parallel to the direction of flow (Tsang and Witherspoon, 1981). The tortuosity of flow paths, introduced by the presence of contact areas forcing the fluid to circulate around them, is not taken into account. For fractures with a small percentage of contact area, the generalized cubic law may be a good formula to describe the flow through a variable-aperture fracture. Recent numerical experiments with random flow-path-network simulations show that the generalized cubic law overestimates the fracture conductivity for fractures with a high percentage of contact area (Tsang, 1984). The tortuosity of flow within a rough fracture becomes an important factor in determining fracture conductivity, and additional resistance due to the presence of large contact areas must be taken into account. In this study, we assume that in the portions of the fractures away from the immediate vicinity of contact areas, the average flow through the open channels can still be described by $\langle b^3 \rangle_1$.

As the fracture desaturates under a negative pressure head, h, the portions of the fracture with apertures greater than the saturation cutoff aperture b_S,

$$b_S = - \frac{2\gamma\cos\theta}{\rho g h} , \qquad (6)$$

will be dry and unable to transmit liquid flow. The dry portions with large apertures are likely to be located away from the contact areas, with the water remaining around the contact areas. Figure 2 shows schematically the changes of liquid-phase configuration on a fracture surface plane during the desaturation process. If the liquid phase is continuous (Figure 2, top), the liquid can flow along the fracture plane with an effective width of flow determined by the width of the neck (W_S in Figure 2) between nearest-neighbor dry areas (air pockets). The ratio of neck width, W_S, to the nearest-neighbor distance, W, can be quantified as an effective phase-separation constriction factor to take into account the blockage of flow by the air pockets and the change of flow paths in swinging around these dry areas.

For the particular geometry shown in Figure 2, the phase-separation constriction factor $\tau = W_S/W$ can be determined by the root of the equation

$$\tau + (1 + \tau^2)\left(\frac{\pi}{4} - \tan^{-1}(\tau)\right) = \sigma \qquad (7)$$

where σ is the effective fraction of area occupied by the liquid water and contact areas (see Figure 3 for the deviation of this formula). If σ is less than $\pi/4$, the liquid phase is discontinuous on the fracture surface and liquid cannot flow along the fracture (Figure 2, bottom). Therefore, $\sigma = \pi/4$ or $\tau = 0$ determines the cutoff for fracture flow for a partially saturated fracture (Figure 2, middle).

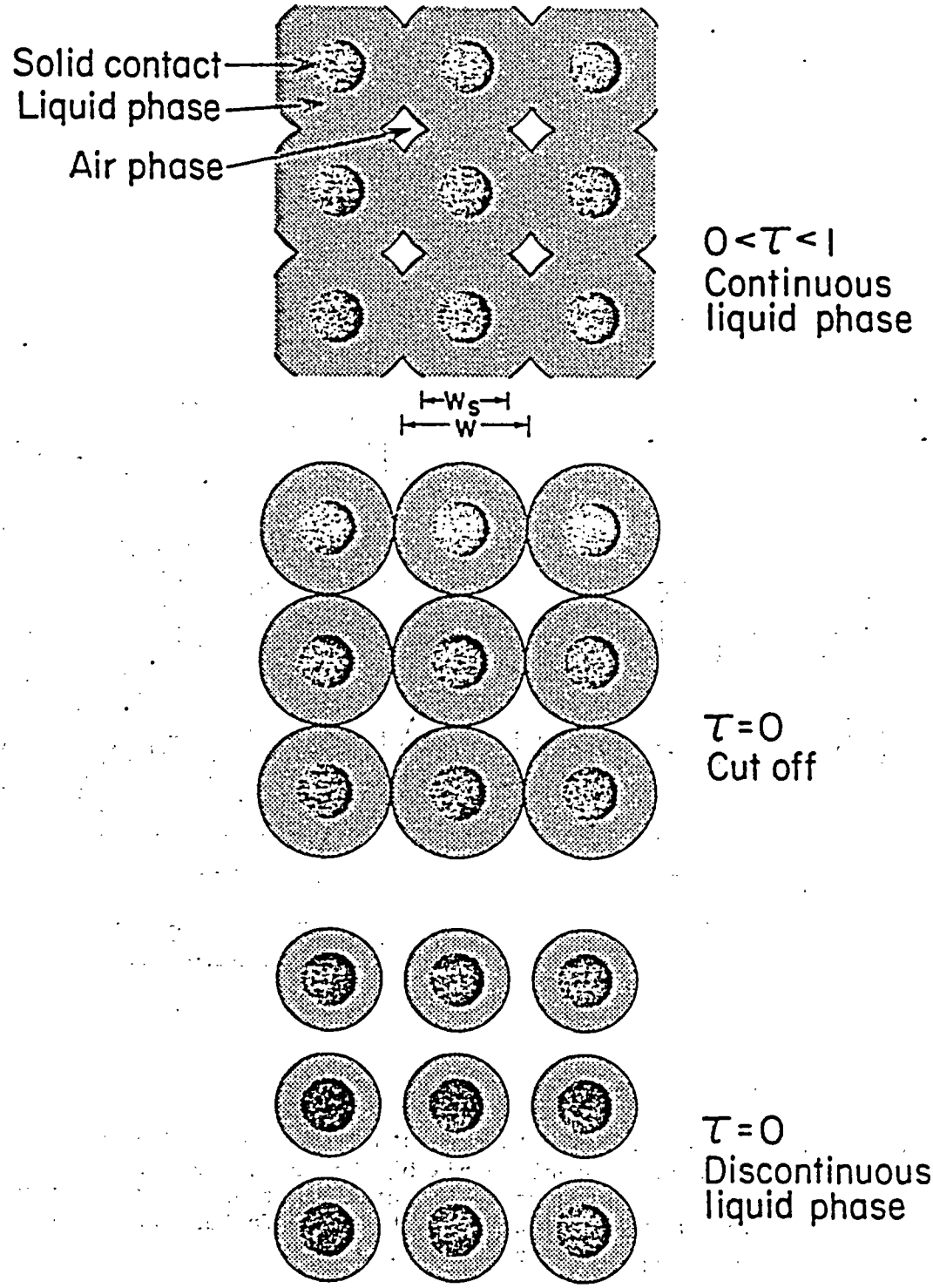

XBL842-9615

Figure 2. Desaturation of fracture surface showing schematically the changes in the fracture plane of liquid-phase (shaded areas) configuration from continuous phase at high saturation (top) to discontinuous phase at low saturation (bottom) with liquid forming rings around contact areas (blackened areas). At the cutoff transition (middle), the ratio τ of the liquid flow path W_S to nearest-neighbor air-pocket separation W is zero (see Figure 3 for a unit area around one contact).

$$\tan\theta = \frac{W_s}{W} = \tau$$

$$R = \sqrt{\left(\frac{W_s}{2}\right)^2 + \left(\frac{W}{2}\right)^2}$$

$$4 \times \frac{1}{2}\left(W_s \times \frac{W}{2}\right) + \pi R^2 \left(\frac{2\pi - 8\theta}{2\pi}\right) = W^2\sigma$$

$$\tau + (1 + \tau^2)\left(\frac{\pi}{4} - \tan^{-1}\tau\right) = \sigma$$

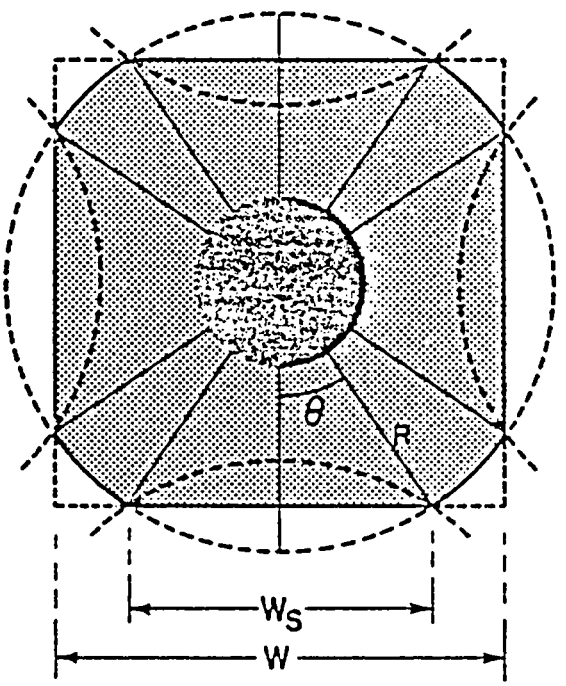

XBL842-9612

Figure 3. A unit area within a fracture plane around a contact area between adjacent matrix blocks (blackened area) surrounded by liquid (shaded area) and air (clear areas in the corners). The phase-separation constriction factor, τ, is derived based on geometric calculations.

Within the liquid phase away from the immediate vicinity of contact areas, the effective average cube aperture is

$$\langle b^3 \rangle_S = \int_0^{b_S} b^3 \, f(b) \, db \quad . \tag{8}$$

The relative permeability for the fracture, defined as the ratio of conductivity at saturation S to that at saturated condition S = 1, is therefore

$$k_r(h) = \tau \frac{\langle b^3 \rangle_S}{\langle b^3 \rangle_1} \quad . \tag{9}$$

The saturation of the fracture is determined by the fraction of fracture opening occupied by the liquid water. Since the averaging over apertures is equivalent to areal integration over fracture surface planes and since fracture volume is the product of aperture and area, we have

$$S(h) = \frac{\langle b \rangle_S}{\langle b \rangle_1} \quad . \tag{10}$$

Flow from the matrix into the fracture and through the fracture into the next matrix block can occur only in the saturated sections and in the contact areas. Since sections with apertures less than the saturation cutoff aperture b_S will be saturated, the effective fraction of area for fracture-matrix flow is

$$\sigma(h) = \omega + \int_0^{b_S} f(b) \, db \quad . \tag{11}$$

Equations 9, 10 and 11 can be used to determine k_r, S, and σ for any given aperture distribution. No data are available for tuff to determine the aperture distribution functions $n(b_o)$ or $f(b)$. Recent analysis of natural

granite fractures shows that $n(b_o)$ takes on a skewed shape, with long tails toward large apertures (Tsang, 1984). A one-parameter distribution, the gamma distribution, could fit the aperture measurements well. The gamma distribution is simply

$$n(b_o) = \beta^2 b_o \, e^{-\beta b_o} \quad \text{or} \quad f(b) = \beta^2 (b+b_c) \, e^{-\beta(b+b_c)} \tag{12}$$

With this simple functional form, analytic expressions for the fracture relative permeability, k_r, saturation, S, and effective fracture-matrix flow area, σ, can be derived:

$$\langle b^3 \rangle_1 = \frac{6(4 + \beta b_c)}{\beta^3} \exp(-\beta b_c) \tag{13}$$

$$k_r(h) = \tau \cdot \frac{1}{6(4 + \beta b_c)} \left\{ \left[24 - \exp(-\beta b_S) \, (24 + 24\beta b_S + 12\beta^2 b_S^2 + 4\beta^3 b_S^3 + \beta^4 b_S^4) \right] + \beta b_c \left[6 - \exp(\beta b_S) \, (6 + 6\beta b_S + 3\beta^2 b_S^2 + \beta^3 b_S^3) \right] \right\} \tag{14}$$

$$S(h) = \frac{1}{2 + \beta b_c} \left\{ \left[2 - \exp(-\beta b_S) \, (2 + 2\beta b_S + \beta^2 b_S^2) \right] + \beta b_c \left[1 - \exp(-\beta b_S) \, (1 + \beta b_S) \right] \right\} \tag{15}$$

$$\sigma(h) = 1 - \exp(-\beta b_c - \beta b_S) \, (1 + \beta b_c + \beta b_S). \tag{16}$$

where the contact cutoff aperture, b_c, is determined by the root of the equation

$$1 - \exp(-\beta b_c) \, (1 + \beta b_c) = \omega. \tag{17}$$

The parameters β and b_c are determined from available tuff properties discussed in the next section.

PROPERTIES OF THE TOPAPAH SPRING MEMBER

To model fluid flow through partially saturated, fractured, porous tuff of the Topopah Spring Member, we used data on discrete fractures, fracture network, and matrix properties. The data are provided by SNL (Hayden et al., 1983), supplemented by data in the literature. For those properties needed for the simulation, but not yet available, the formulae presented in this report were used. All parameters in the formulae were determined by the data. The formulation and statistical theory in this report can accommodate detailed fracture and matrix data, and no adjustable parameter needs to be introduced in the simulations.

Matrix Data

The data are mainly from laboratory measurements of core samples from different boreholes at Yucca Mountain:

- o matrix saturated permeability 3.26×10^{-17} m^2 or 3.2×10^{-8} cm/sec from borehole USW-GU3,
- o matrix saturation 0.8 or 80%, from boreholes USW-GU3 and USW-G4,
- o matrix characteristic curve

$$S = (1 - S_r)\left[\frac{1}{1 + |Ah|^{\beta}}\right]^{(1 - \frac{1}{\beta})} + S_r \quad , \text{ and} \tag{18}$$

- o matrix relative permeability

$$\frac{k_m(S)}{k_m(1)} = \left[1 + |Ah|^{\beta}\right]^{-\lambda/2}\left\{1 - \left[\frac{|Ah|^{\beta}}{1 + |Ah|^{\beta}}\right]^{\lambda}\right\}^2 \tag{19}$$

where $S_r = 9.6 \times 10^{-4}$

$A = 7.027 \times 10^{-3}$ 1/m

$B = 1/0.45 = 1.818$

$\lambda = 1 - 1/B = 0.55$.

These values were obtained by a least square fit (Hayden et al., 1983) to the empirical data from borehole USW-GU3 with the equation used by van Genuchten (1980). In our simulations, the matrix saturation was varied between the fully saturated condition, $S = 1$, and the matrix saturation, $S = 0.8$, a range far away from the residual saturation, S_r, which usually is poorly measured and poorly fitted. The relative permeability formula is derived from the characteristic curve formula by van Genuchten (1980) following the theory of Mualem (1976).

Fracture Network Data

Fracture patterns, orientations, and spacings have been measured in borehole cores and from surface mapping. The fracture data of the Topopah Spring Member (Spengler and Chornack, 1984) from borehole USW-G4 include:

- o apparent fracture frequency, $f = 4.36$/m, and
- o distribution of fracture inclination (dipping angle between 0° and 90°) as shown in Figure 4.

Figure 4 shows that the fracture inclinations in the densely welded Topopah Spring Member may be grouped into two catagories. 56% of the fractures have steeply dipping inclinations (>45°) and can be classified as nearly vertical. 44% of the fractures have small inclinations (<45°) and may be classified as nearly horizontal. The averages of the cosine of the dip angles for each group in the distribution of Figure 4 are:

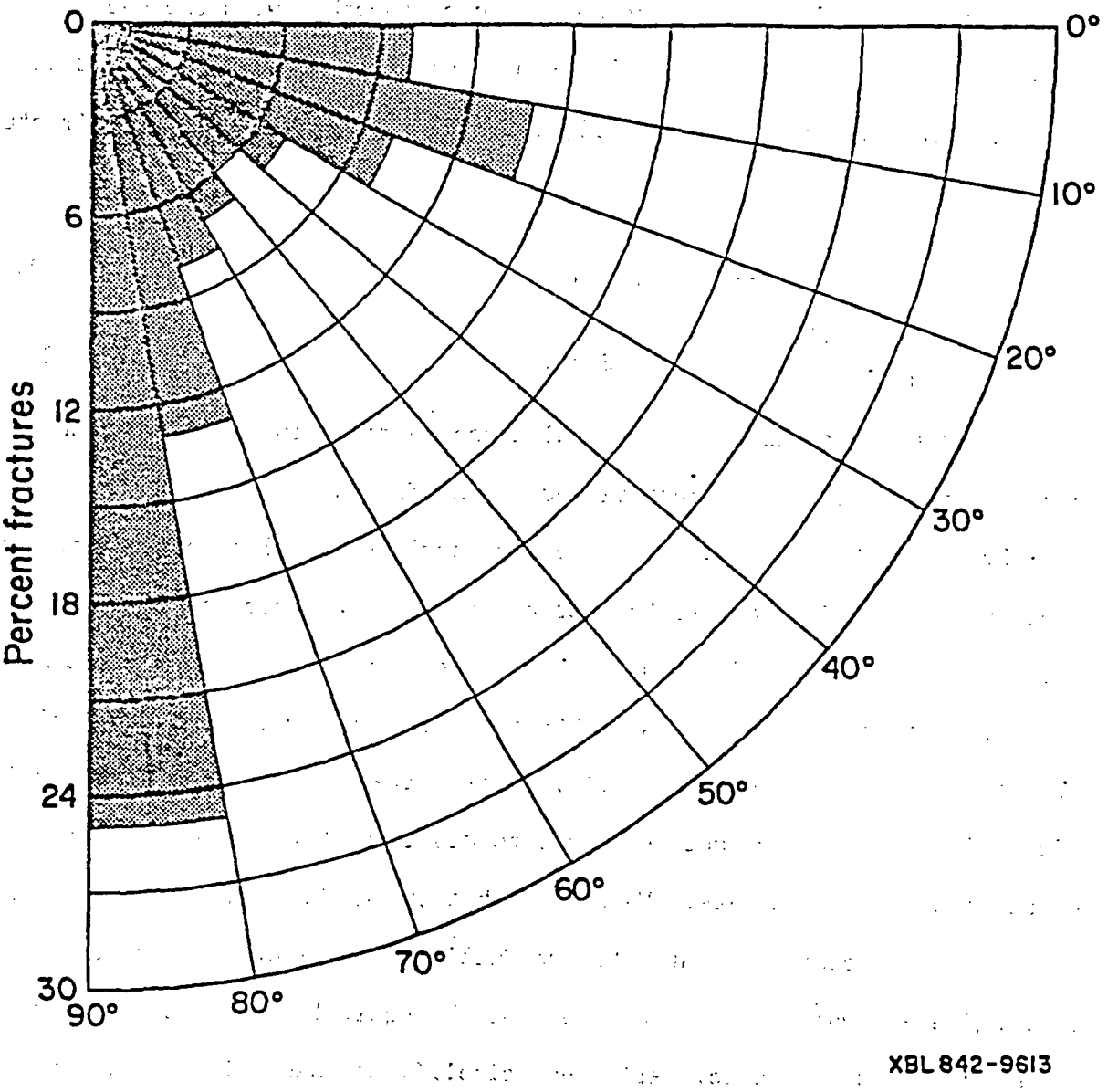

Figure 4. Inclination of fractures in the densely welded Topopah Spring Member (from Spengler and Chornack, 1984).

$$\langle COS \rangle_V = 0.27 \tag{20}$$

$$\langle COS \rangle_H = 0.92 \ . \tag{21}$$

The subscripts V and H represent the nearly vertical and nearly horizontal groups, respectively. These cosine averages, together with the overall apparent fracture spacing of f = 4.36/m in borehole USW-G4, were used to determine the spacings of the nearly vertical and nearly horizontal fracture sets:

$$D_V = \frac{\langle COS \rangle_V}{f} = 0.22 \text{ m} \tag{22}$$

$$D_H = \frac{\langle COS \rangle_H}{f} = 0.48 \text{ m} \ . \tag{23}$$

These spacings were used in the simulations to determine the dimensions and size of the matrix blocks partitioned by the fractures.

From surface mapping, there are two nearly vertical fracture sets dipping steeply (60° - 90°); one strikes north-northwest, one strikes north-northeast (Scott et al., 1982). The NNW set has higher density but may tend to have smaller apertures than those with NNE trends. The regional stress field is oriented with the maximum horizontal compressive stress in the NE direction (Carr, 1974). Data are not available to distinguish between the hydraulic properties of the two sets. We assume that the contributions from each set to the equivalent continuum saturated conductivity (cube of aperture divided by spacing) are equal. We also assume that the equivalent fracture continuum conductivity is isotropic. All these simplifying assumptions about the fracture network can be relaxed easily when additional and more detailed field data become available.

Along a given direction in three-dimensional space, two fracture sets contribute to the equivalent continuum conductivity, k_f. We have

$$\frac{k_f}{2} = \frac{\langle b^3 \rangle}{12D} \tag{24}$$

for each set with spacing D.

The interconnection of fractures in the welded tuff is demonstrated by hydrologic tests near Yucca Mountain, which shows that the volume of water removed during pumping tests is much greater than the volume of the fractures close to the drill holes (Thordarson, 1983). The several orders of magnitude difference between the laboratory measurements of matrix permeability and the field measurements of in situ permeability, discussed in the next paragraph, supports the assumption that fractures form a continuous, connected network that provides an effective pathway for fluid movement under saturated conditions.

Fracture Permeability

The data base for fracture permeability is taken from results of a performance assessment working group (PAWG) meeting held in San Francisco in June, 1983 (Tyler, 1983):

- fracture continuum saturated permeability $k_f = 1.02 \times 10^{-11}$ m^2 or 10^{-2} cm/sec (range 10^{-2} - 10^{-4} cm/sec).

This fracture saturated conductivity is deduced from well testing in well J-13 and is assumed to represent the equivalent fracture continuum (S. Sinnock, SNL, personal communication, October, 1983; Thordarson, 1983). Well J-13 is located in a low-standing structural block with part of the Topopah

Spring Member saturated. The high in situ conductivity of the Topopah Spring Member in Well J-13 may be caused in part by the presence of faults and associated fractures. In the NTS, highly fractured, densely welded tuffs have effective hydraulic conductivities that are approximately 5 or 6 orders of magnitude larger than the matrix hydraulic conductivities (Winograd and Thordarson, 1975). However, knowledge of hydrologic properties of unsaturated units at Yucca Mountain is incomplete. Preliminary analysis of air permeability tests on borehole UE25a-4 indicates that the densely welded Topopah Spring Member may be more conductive than the values quoted by Winograd and Thordarson (1975) (P. Montazer, USGS, personal communication in environmental assessment planning meeting, October, 1983). We tentatively chose 10^{-2} cm/sec as the saturated value of hydraulic conductivity k_f of the fracture continuum. This parameter is one of the most important hydrologic data in determining the flow field at Yucca Mountain.

Discrete Fracture Data

The data for fracture surface roughness and aperture distributions are being measured, but are not yet available. We used indirect data from analysis of core from borehole USW-G4 (Spengler and Chornack, 1984) that indicates:

- Fracture coatings $\omega = 12\%$ with zeolites, clay, calcite.

The fraction 12% of fracture area with coatings is assumed to correspond to the fraction of in situ contact area between matrix blocks. The identification of fracture coatings with contact area is a novel assumption. Further study will examine the credibility of this identification. The contact area

can also be determined independently with flow-stress-fracture-displacement measurements. For granite and basalt, the fractional contact areas at 20 MPa normal stress are in the range of 15 - 20%. (Tsang and Witherspoon, 1981; Iwai, 1976). The fractional contact area of 12% for tuff, based on the assumption that hydrochemical alterations occur in contact areas which remain at continuous contact with water for a long time, may be a reasonable estimate.

FRACTURE SATURATION, PERMEABILITY, AND EFFECTIVE FRACTURE-MATRIX FLOW AREA

With the available data and explicit formulae derived for the gamma aperture distribution, the partially saturated fracture properties as functions of negative pressure head can be calculated and used in the TRUST program. In summary, the calculational steps are:

(1) With $\omega = 12\%$, βb_c is determined by Eq. 17.

(2) With $k_f = 1.02 \times 10^{-11}$ m^2 $= 10^{-2}$ cm/sec, and spacing D_V, D_H of Eqs. 22, 23, the β's are determined by:

$$\beta^3 = \frac{(4 + \beta b_c) \exp(-\beta b_c)}{D k_f} \tag{25}$$

The results are

$$\beta_V = 1.04 \times 10^4 \text{ 1/m} , \tag{26}$$

$$\beta_H = 0.804 \times 10^4 \text{ 1/m} . \tag{27}$$

The aperture distribution functions with these distribution parameters are plotted in Figure 5. The contact cutoff aperture, b_c, is derived to be 0.057 mm for the vertical fractures and 0.074 mm for the horizontal fractures. The average apertures, defined as the cubic root of the cube average, $[\langle b^3 \rangle_1]^{1/3}$, are

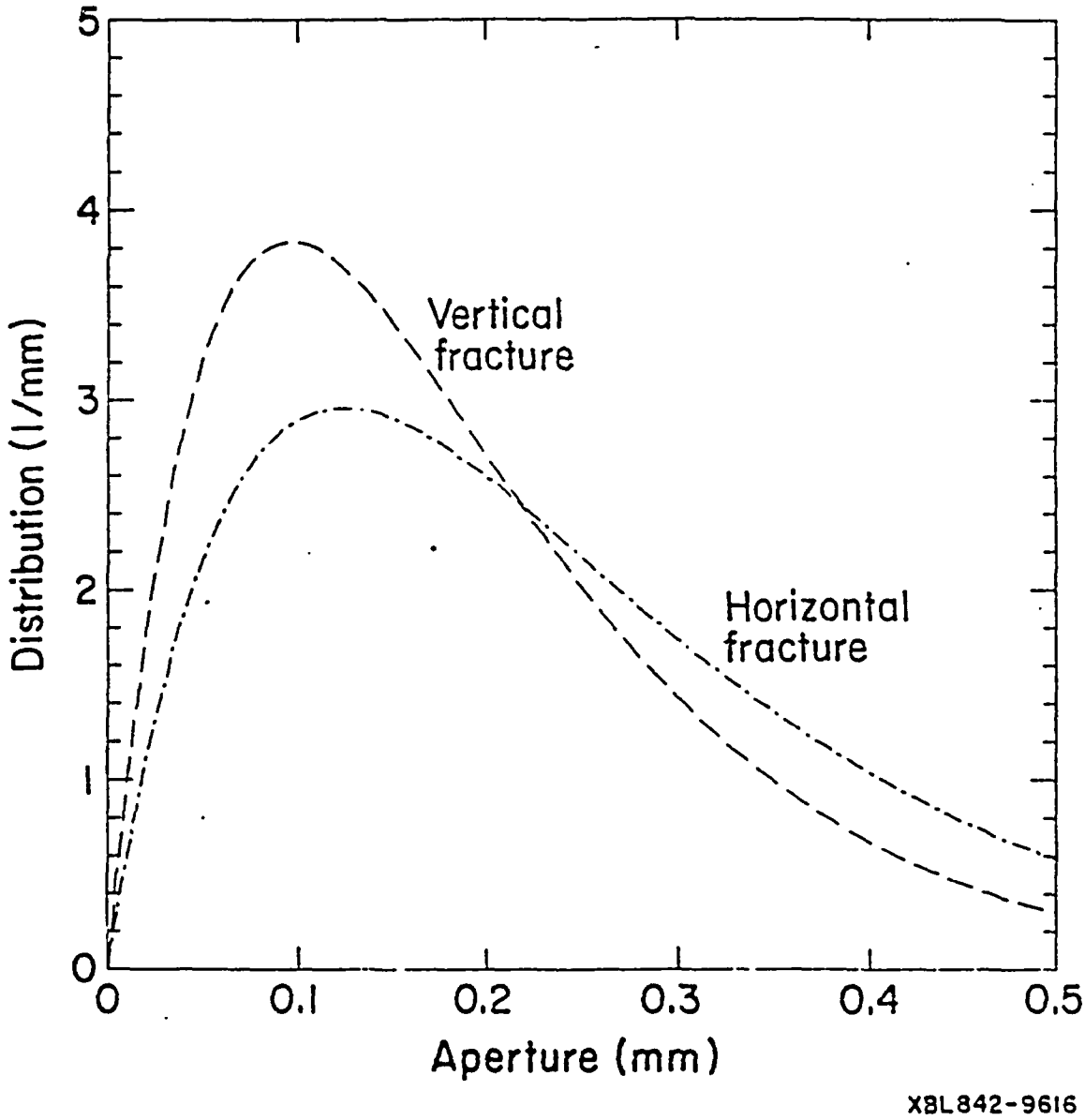

Figure 5. Gamma aperture distributions of vertical and horizontal fractures with distribution parameters derived from Topopah Spring Member data.

$$\bar{b}_V = 0.24 \text{ mm} \tag{28}$$

$$\bar{b}_H = 0.31 \text{ mm} \quad . \tag{29}$$

(3) With b_S given by Eq. 6, and the formulae of Eqs. 14, 15 and 16, the fracture saturation, discrete fracture permeability, $k_r\bar{b}^2/12$, and effective fracture-matrix flow area can be calculated as functions of negative pressure head. These relationships are plotted in Figures 6, 7, and 8. The matrix saturation from Eq. 18 and permeability from Eq. 19 are also plotted for comparison.

Figure 6 shows that fractures can desaturate easily with a small suction of -10^{-1} m. The saturation in the matrix will remain high. If the in situ matrix saturation is 0.8, then the negative pressure head in the Topopah Spring Member is -112 m. With such a large suction, the fracture saturations will be essentially zero.

Figure 7 shows that the fracture permeabilities are very sensitive to suction. If fully saturated, the permeability of each discrete fracture is 8 orders of magnitude greater than the matrix permeability. The equivalent fracture continuum permeability is 3.1×10^5 greater than the matrix permeability. With small suctions in the range -10^{-1} to -10^{1} m, the discrete fracture permeabilities decrease drastically. The matrix permeability decreases much more gently as the pressure head becomes more negative. Near fully saturated conditions, the fractures will control the fluid flow. As desaturation proceeds and the fracture permeability of each discrete fracture become less than the matrix permeability, the matrix will control the flow. For in situ suction of -112 m in the Topopah Spring Member, fracture flow is negligible and matrix flow dominates.

Two sets of discrete fracture permeabilities are plotted in Figure 7, one with the phase-separation constriction factor τ of Eq. 7 taken into account,

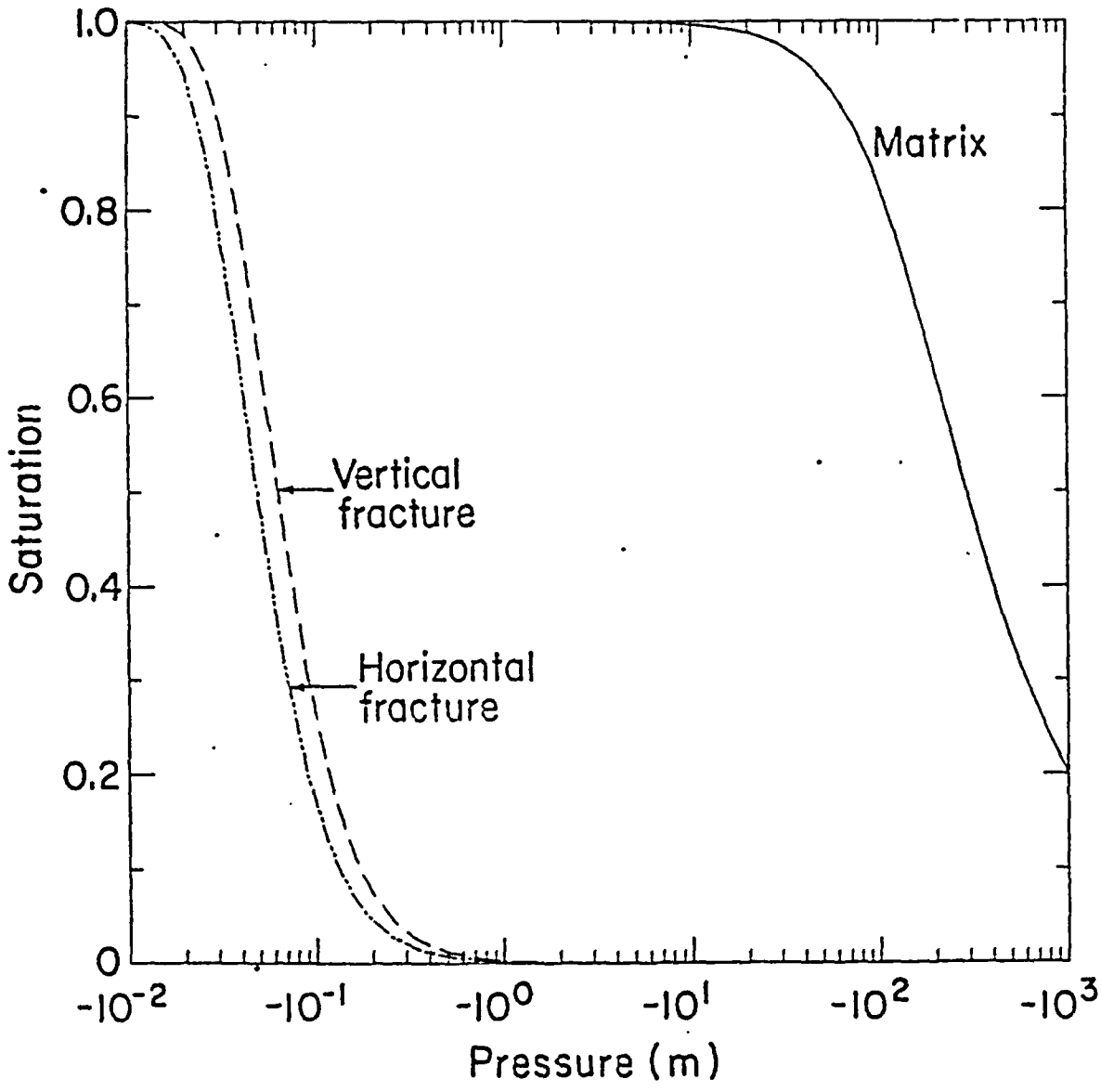

Figure 6. Characteristic curves (saturation vs. head) of vertical fracture, horizontal fracture, and tuff matrix with parameters derived from Topopah Spring Member data.

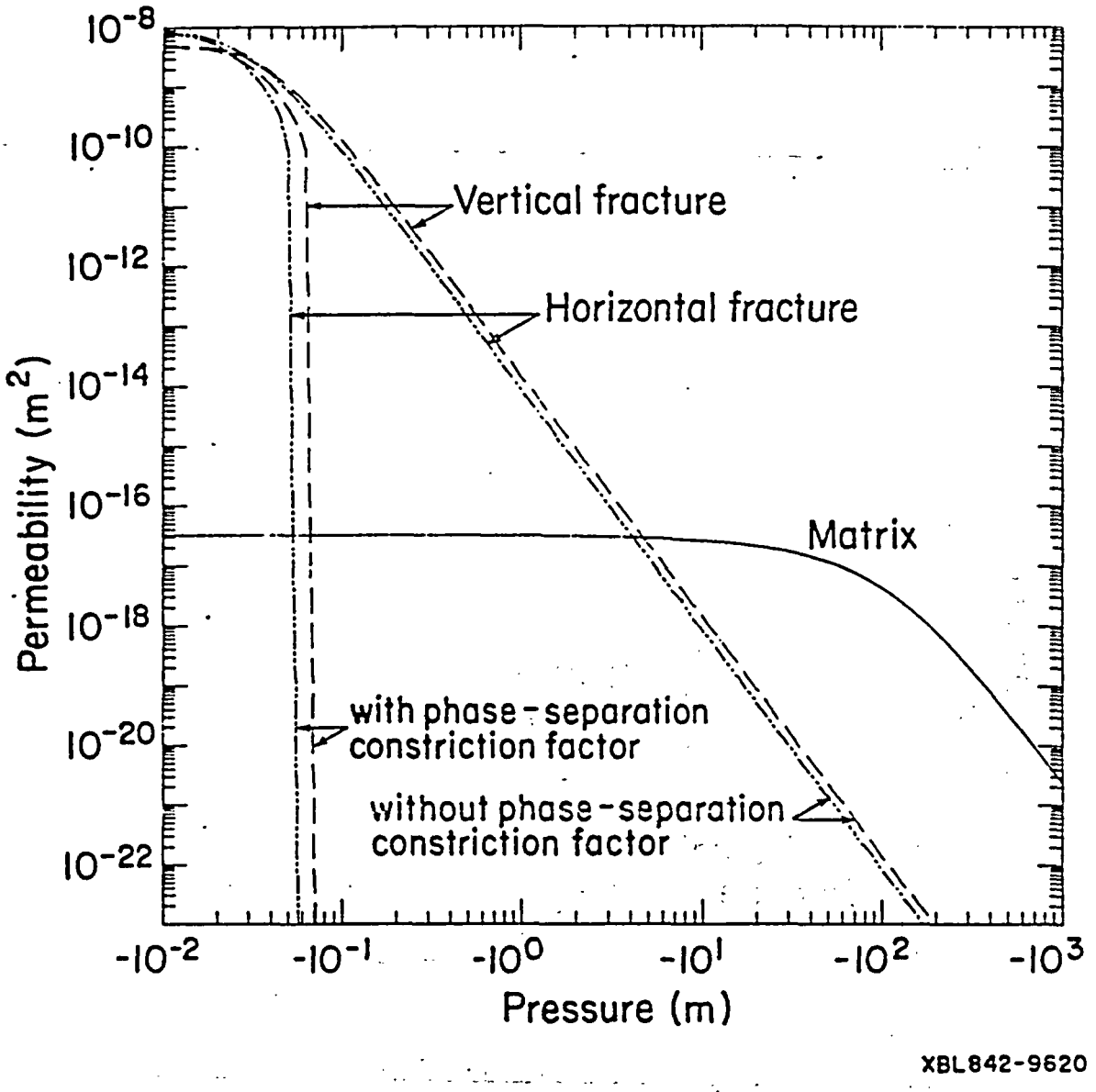

Figure 7. Permeabilities of partially saturated discrete fractures and tuff matrix with parameters derived from Topopah Spring Member data.

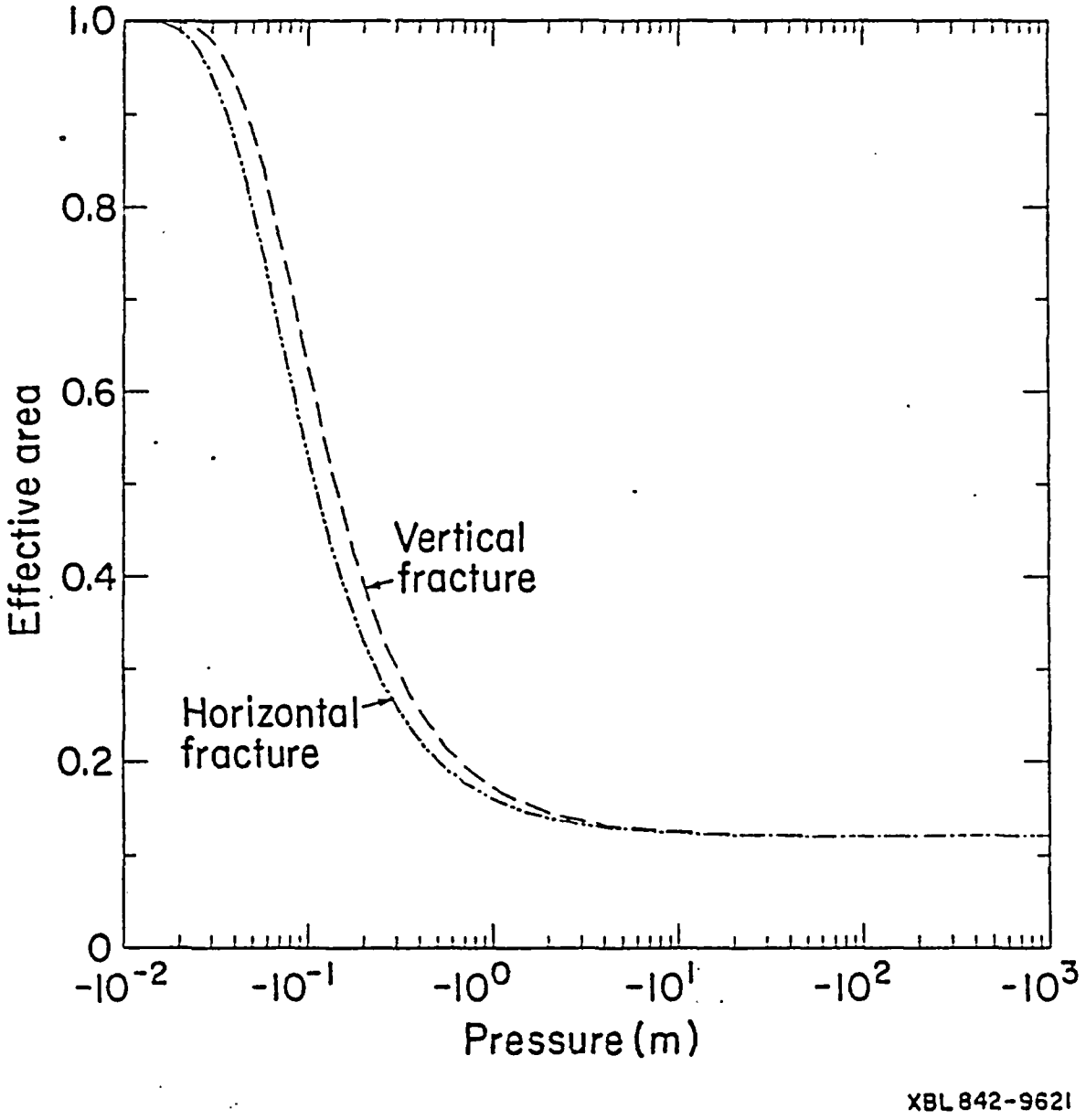

Figure 8. Effective fracture-matrix flow areas at fracture-matrix interfaces with parameters derived from Topopah Spring Member data.

one with $\tau = 1$. The phase-separation constriction factor takes into account the effects of blockage of flow by air pockets, the flow-path distortion around the air pockets, and the presence of a discontinuous liquid phase with fluid remaining stationary around fracture surface contacts. The cases with $\tau = 1$ ignore the blockage effects and take into account only the generalized cubic law for fracture flow. With $\tau = 1$, we overestimate the fracture permeabilities and ignore the fracture permeability cutoff. The effects of this phase-separation constriction factor will be discussed in the simulation results.

The matrix flow also will be impeded when it crosses the fractures. The matrix-fracture flow is limited by the available area on the fracture surfaces where fluid can be transmitted. Figure 8 shows that the effective fracture-matrix flow area decreases and quickly approaches the limiting contact area fraction, ω, as the pressure head decreases. The effective fracture-matrix flow area reduces the available area for matrix flow across the matrix-fracture interfaces. With liquid flow from one matrix block to another restricted to the saturated areas, the flow lines will bunch around asperities and flow paths in a partially saturated, fractured porous medium will be more tortuous than in a fully saturated, fractured porous medium.

TRUST COMPUTER PROGRAM

To implement the conceptual model and statistical formulation, the computer code TRUST (Narasimhan et al., 1978) has been updated in several respects. Additional characteristic curves and relative permeability curves were programmed. The van Genuchten (1980) formulae are needed to simulate the matrix blocks. The gamma distribution formulae will be used

for the discrete fracture grid blocks. Also included are the hyperbolic characteristic curves used by Pickens et al. (1979).

The areas between neighboring nodes are multiplied by a new effective-area factor to account for the changes of flow areas in fracture-matrix connections. Two options are programmed for the effective-area factor: the gamma-distribution effective-area formula or any tabulated data. If experimental data on fracture aperture distributions were available, it may be more convenient to integrate numerically over the measured distribution and generate tabulated data for the effective fracture-matrix flow area.

With the use of extended memory, the modeling capabilities are increased to handle 2500 nodes and 5000 connections. All the arrays which depend on the nodal numbers and connection numbers are grouped together in the main program so that these arrays can be easily re-dimensionalized.

In addition to the efficient iterative solver, TRUST also can use the MA28 package for direct solution of the linear equations with a sparse variant of Gaussian elimination (Duff, 1977). All arrays for the MA28 routine are in large core memory. The direct solver is also used in the new version of the TRUST program to solve the steady-fluid-flow field.

FRACTURED TUFF COLUMN SIMULATIONS

A test case was set up to simulate the fluid flow in partially saturated, fractured, porous tuff. Simulations of vertical drainage within the Topopah Spring Member were performed. Two vertical fracture sets and one horizontal fracture set partitioned the tuff formation into blocks as shown in Figure 9. Figure 9 shows 5X5X3 blocks with each block being 0.22 m x 0.22 m x 0.48 m.

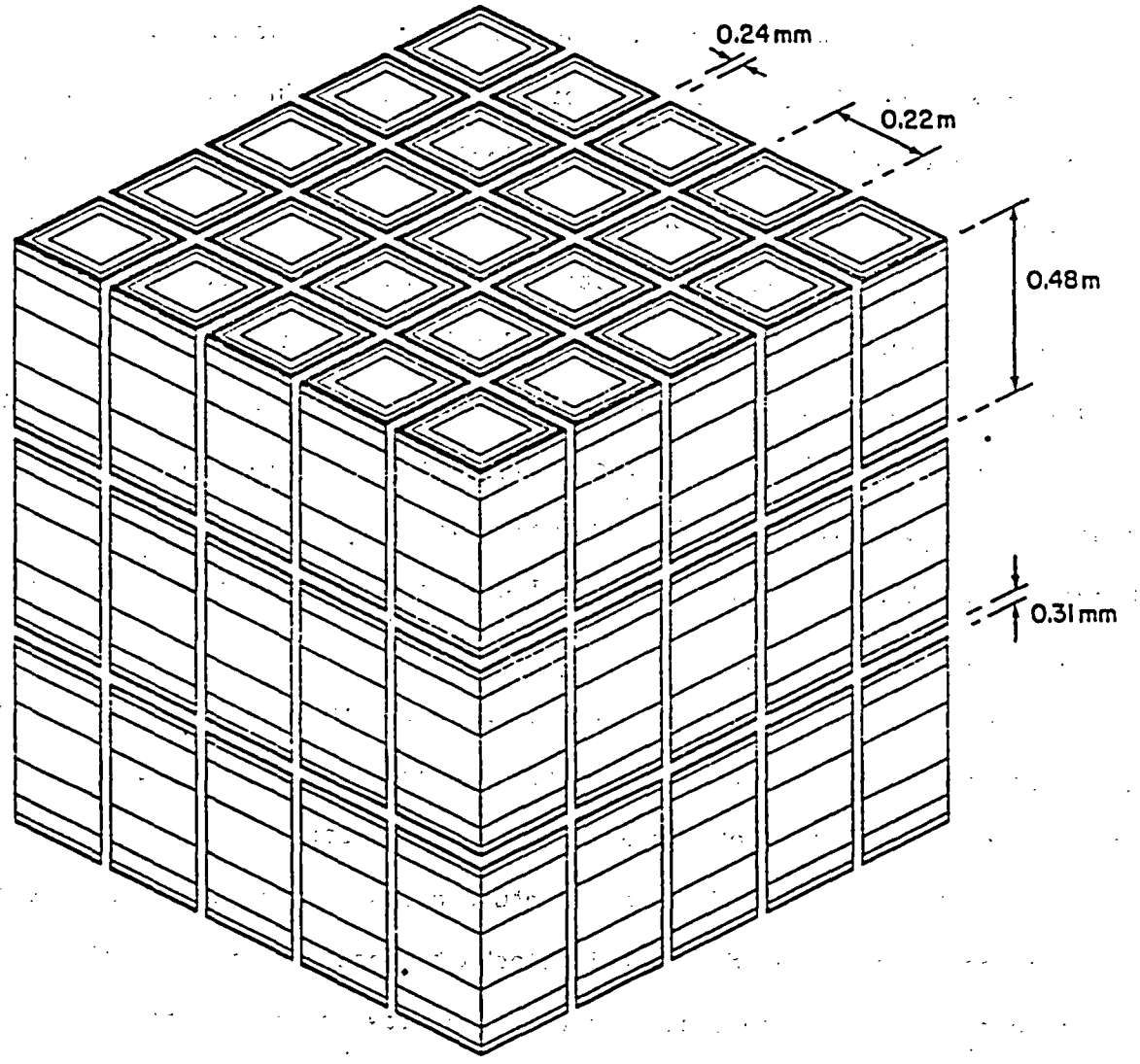

Figure 9. Grid of fractured, porous tuff used to represent the densely welded Topopah Spring Member.

The fracture apertures, 0.24 mm for the vertical fractures and 0.31 mm for the horizontal fractures, are emphasized 100-fold in Figure 9. To simulate vertical drainage, only one vertical column bounded by four vertical fractures needs to be modeled. By symmetry, the midplanes of the bounding vertical fractures are no-flow boundaries. The horizontal fractures, normal to the direction of general flow, are explicitly simulated. On the local scale, lateral flow is allowed between the vertical fractures and the matrix blocks. The horizontal cross section of the column is further partitioned into 6 nested elements and the vertical cross section of each block is sliced into 9 sections (Figure 10). The partition of horizontal nested elements is similar to that used in the MINC program (Pruess and Narasimhan, 1982) without grouping the matrix elements from different blocks together. The grid elements are small near the fractures and large toward the middle of the matrix block as shown in Figure 10 and tabulated in Table 1; 203 elements and 370 connections are used in the grid.

The conductances at the interfaces are determined by the harmonic means of the permeability values of the neighboring nodes weighted by the distances from the node centers to the interfaces. For the connections between the fracture and matrix, the distances from the fracture nodes to the interfaces are set to zero so that normal flow from matrix blocks to fractures is controlled by matrix permeability. The available area for flow across the fracture-matrix interfaces is determined by fracture saturations. At the limit that the fractures are completely desaturated, the available area for matrix flow from one block to the next is the contact area between adjacent blocks. The outermost matrix node for one block is connected to the fracture and is not directly connected to the matrix node in the next block in the simulations.

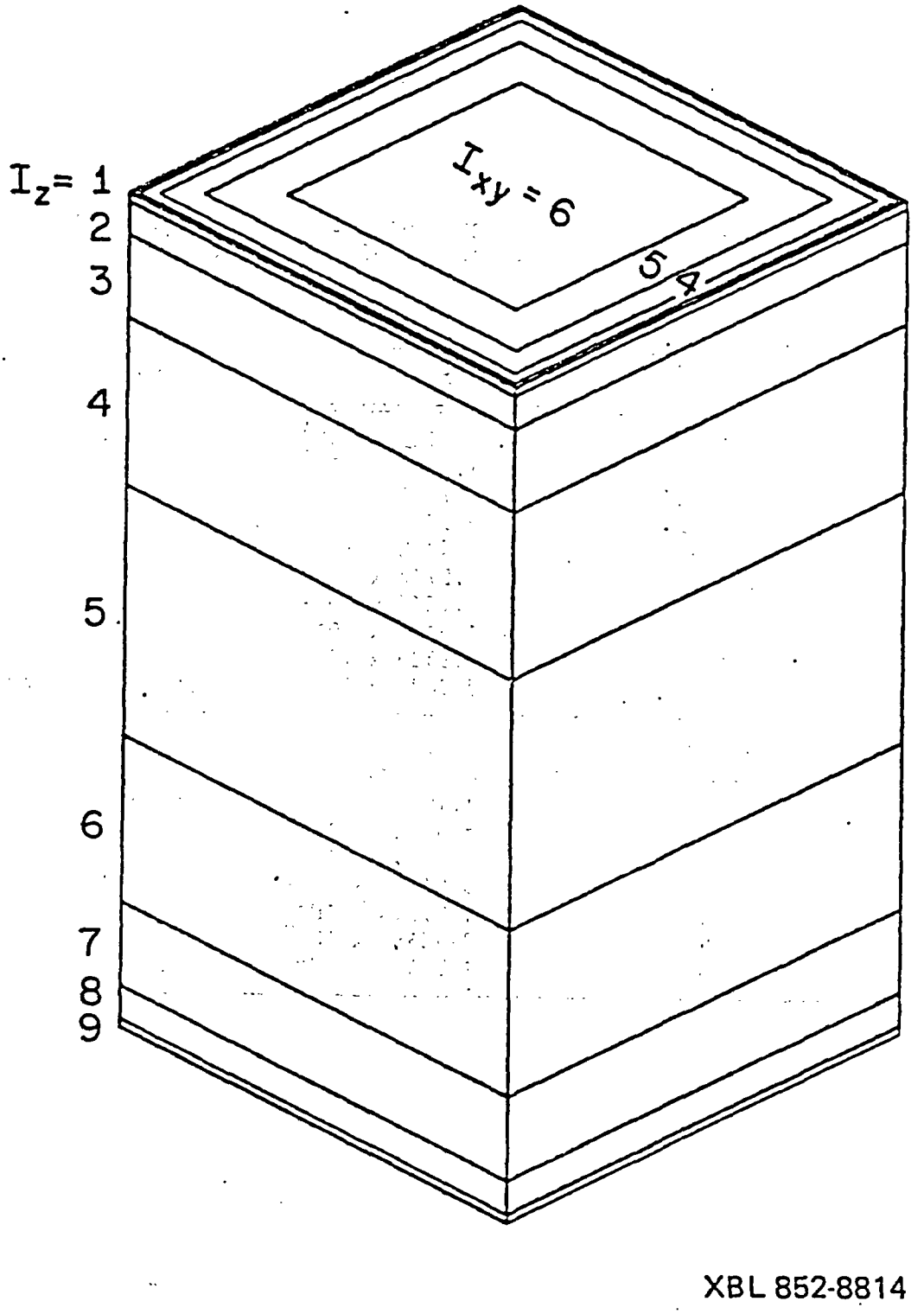

Figure 10. Grid of one matrix block.

Table 1. Spacings of grid used in partially saturated, fractured, porous tuff simulations

Node Index I_z	Δz(m)	Material
1,11,21	4.6325×10^{-3}	Tuff Matrix
2,12,22	1.9146×10^{-2}	"
3,13,23	4.7866×10^{-2}	"
4,14,24	9.5732×10^{-2}	"
5,15,25	1.4360×10^{-1}	"
6,16,26	9.5732×10^{-2}	"
7,17,27	4.7866×10^{-2}	"
8,18,28	1.9146×10^{-2}	"
9,19,29	4.6325×10^{-3}	"
10,20	3.8024×10^{-4}	Horizontal Fracture
Node Index I_{xy}	**Δxy(m)**	**Material**
0	1.19×10^{-4}	Vertical Fracture
1	4.3362×10^{-4}	Tuff Matrix
2	2.2394×10^{-3}	"
3	5.8140×10^{-3}	"
4	1.27614×10^{-2}	"
5	2.3666×10^{-2}	"
6	1.3033×10^{-1}	"

The upper boundary is a no-flow boundary. The lower boundary is a constant suction boundary. The suction head is maintained at -112 m, the in situ suction. Initially the system is fully saturated with pressure determined by hydrostatic equilibrium. The potential everywhere is zero, and fluid is stationary. At $t = 0^+$, the negative suction head at the lower boundary begins to induce transient changes in the fluid-flow field throughout the fractured, porous tuff column. The TRUST program automatically controls the time steppings and iterations of nonlinear fracture and matrix properties. For the full simulations of the fractured-matrix drainage over a time span of 10^5 years the program requires 42 CPU sec on Lawrence Berkeley Laboratory's CDC7600 computer.

Five cases of flow in fractured, porous tuff were studied: (1) a fractured, porous column with the phase-separation constriction factor taken into account ($0 \leq \tau(h) \leq 1$) (2) a fractured, porous column without phase-separation constriction factor ($\tau = 1$), (3) a matrix column without fractures, (4) a discrete fracture network without matrix and with τ factor and (5) a discrete fracture network without matrix and without τ factor. The results are presented in plots of pressure head, saturation, permeability, effective fracture-matrix flow area, and Darcy velocity versus time at different locations (Figures 11-16). The locations of interests are the middle of the matrix block (point A), the middle of the vertical fracture (point B), the middle of the upper horizontal fracture (point C) and the middle of the lower horizontal fracture (point D) as shown in the inserts of the plots. We also plotted the velocities at the matrix-fracture interfaces at these mid-points and along the fractures at the fracture intersections.

Pressure Drop

Figure 11 shows the pressure drop at different locations in response to the negative suction at the lower boundary. The pressure heads decrease from the initial positive hydrostatic pressure and become negative at 10^{-5} years for Case 1, and the pressure heads decrease more gradually at earlier times for Case 2. After the pressure drop at 10^{-5} years for Case 1, a small but noticeable increase in pressure is observed in the simulated results before large decreases at later times.

As pressures become negative following initial desaturations, the pressure changes are controlled mainly by the matrix. Cases 1, 2, and 3 are essentially the same after 10^{-2} years. The lower fracture, Point D, is closer to the suction boundary and has more negative pressure than the higher elevation points. At the same elevation, the matrix pressure at Point A and the vertical fracture pressure at Point B are approximately the same. Therefore, pressure changes can be simulated with matrix properties only, if the transition from saturated conditions to unsaturated conditions is not of interest.

Very different results are obtained if the changes in a fractured-porous system are simulated only through the discrete fracture network (Cases 4 and 5 in Figure 11). Taking into account the phase-separation constriction effects (Case 4), the fractures remain at pressures near zero during the entire simulation period of 10^5 years. If the phase-separation constriction factor is not taken into account (Case 5), the fractures will respond to the negative suction, but at extremely long times as a result of the highly nonlinear fracture characteristic curves. Without the presence of matrix blocks to act as flow channels for fluid to change pressures, unrealistic results are obtained.

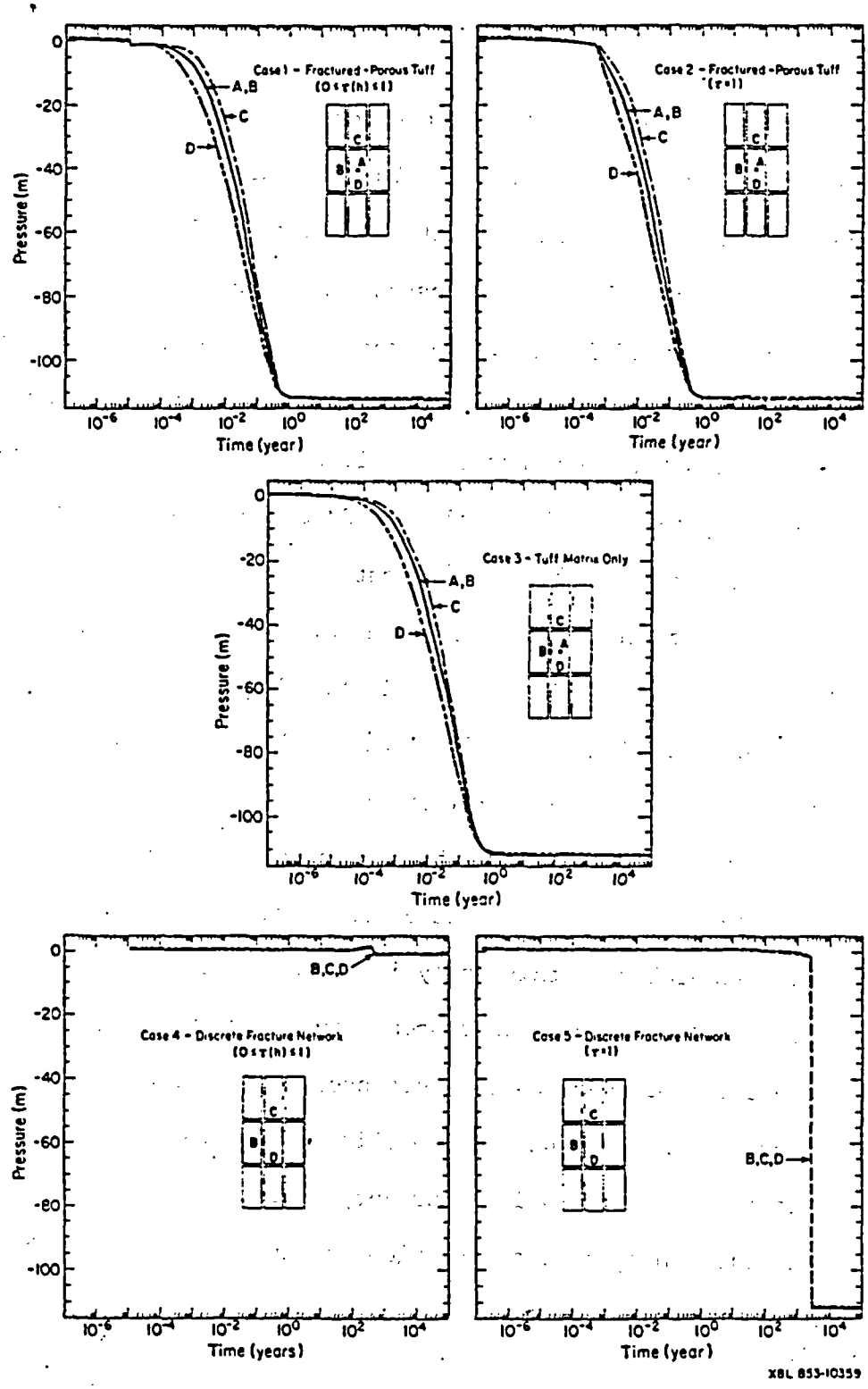

Figure 11. Pressure drops at discrete points during drainage of a fractured tuff column.

Saturation Change

Figure 12 illustrates the saturation changes at different points for the five cases. In Cases 1 and 2 for the fractured, porous tuff column, the fracture saturation drops abruptly at early times. The matrix changes more slowly from the initial fully saturated condition of S = 1 to the final ambient saturation of S = 0.8. The desaturation of fractures is sensitive to the phase-separation constriction factor. In Case 1 and Case 4 with $0 \leq \tau(h) \leq 1$, the saturation changes at different fracture locations occur essentially at the same time while for Case 2 and Case 5 with $\tau = 1$, the upper horizontal fracture (Point C) desaturates first, followed by desaturation at the vertical fracture (Point B) of middle elevation, and the lower horizontal fracture (Point C) desaturates last. Case 4 in Figure 12 shows that fracture saturation drops from S = 1 to nearly S = 0 with the small pressure changes illustrated in Case 4 of Figure 11.

The rates of the simulated saturation changes shed light on the feasibility of laboratory studies of fractured-tuff properties. For the 1.44-m-long tuff column simulated in this analysis, a change in matrix saturation of $\Delta S = 0.2$ requires 10^{-2} to 1 year in response to the suction on the lower boundary. If experiments were carried out over shorter time spans, the observation of saturation changes would be unreliable. On the other hand, saturation changes in the fractures will occur very abruptly. Therefore, instruments to detect saturation changes must have high resolution to detect the occurrence of the desaturation processes.

Permeability Change

Figure 13 shows the permeability changes at different points for the five cases. The permeability changes illustrate even more drastically than

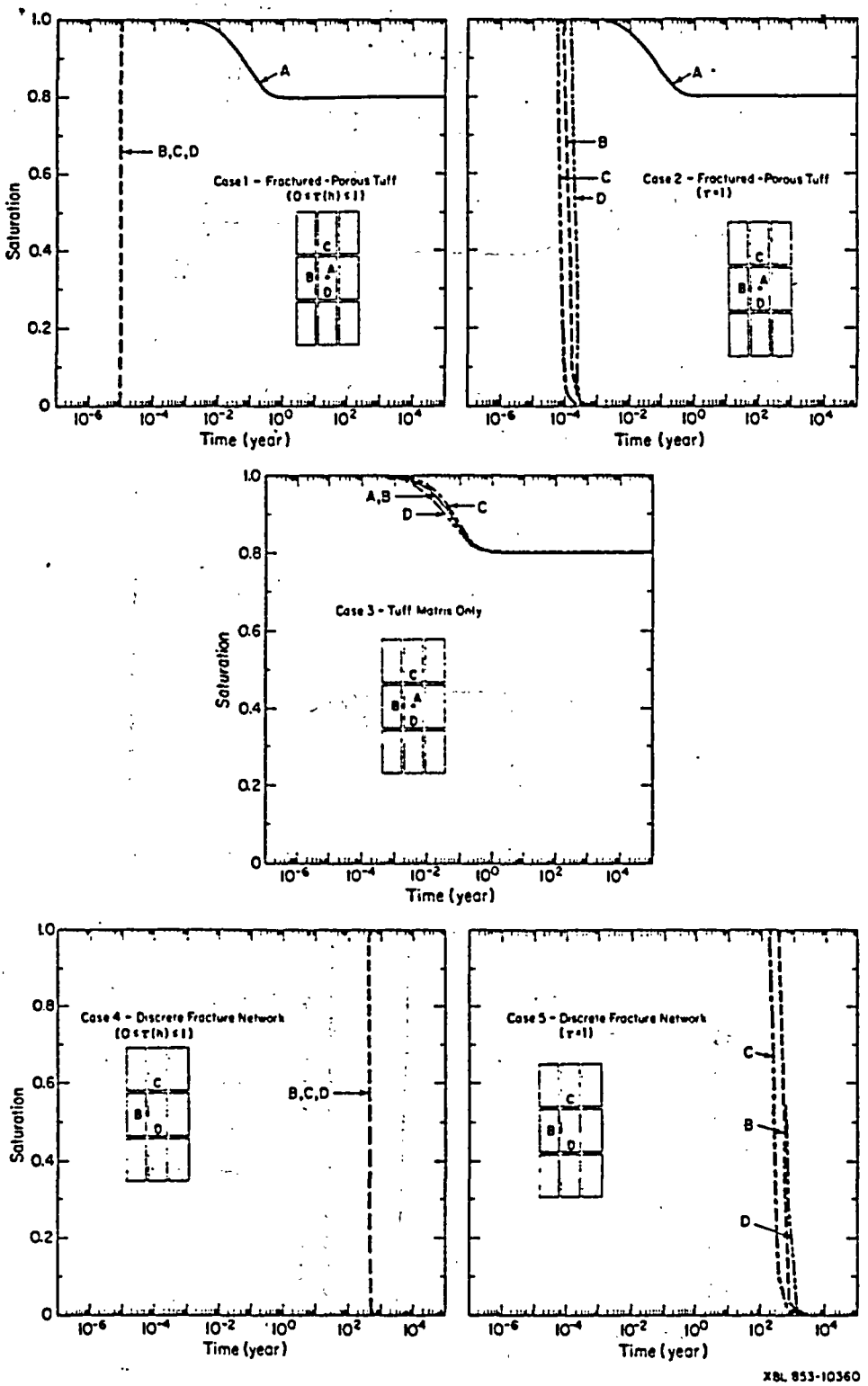

Figure 12. Saturation changes at discrete points during drainage of a fractured tuff column.

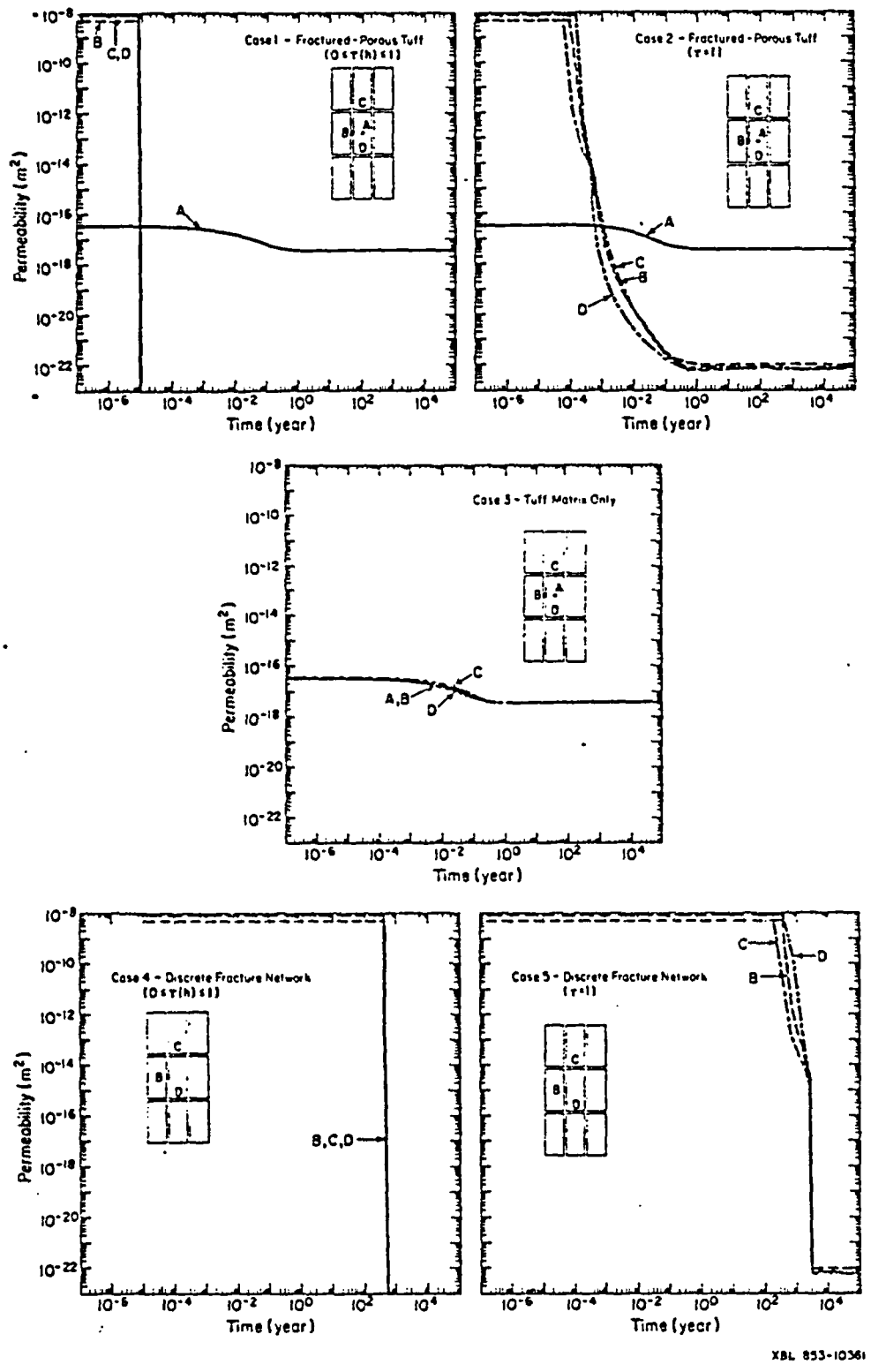

Figure 13. Permeability changes at discrete points during drainage of a fractured tuff column.

the saturation changes the contrast in behavior between fractures and porous matrix. Case 1 indicates that fractures will stop transmitting fluid 10^{-5} years after the suction begins. The matrix permeability changes by less than an order of magnitude from the initial condition of S = 1 to the final condition of S = 0.8. Initially the fracture permeabilities of each discrete fracture are more than 8 orders of magnitude greater than the matrix permeability. The fracture permeability changes are sensitive to the phase-separation constriction factor as shown in the difference between Case 1 with $0 \leq \tau(h) \leq 1$ and Case 2 with $\tau = 1$. For Case 2, the fractures will remain conductive at the final ambient conditions with the permeabilities more than 4 orders of magnitude smaller than the matrix permeability. However, Case 2 with $\tau = 1$ does not account for the possibility that the liquid phase may become discontinuous, thereby blocking flow.

Effective Fracture - Matrix Flow Area Change

Figure 14 illustrates the changes in the effective area at the midpoints of fractures for flow across the matrix-fracture interfaces for Case 1 and Case 2. As the fractures desaturate, the wetted area on the fracture surfaces decreases. At complete desaturation, only the contact area, which is $\omega = 12\%$ of fracture surface in these simulations, is available for fluid flow from one matrix across fractures to the next matrix block. This reduction in effective fracture-matrix flow area may significantly change the actual flow paths for fluid movement.

Darcy Velocity Changes in Fractures

Figure 15 illustrates the changes in Darcy velocities at the fracture intersections for Case 1 and Case 2. Before the fractures desaturate, fluid mainly flows downward along the vertical fractures. The downward

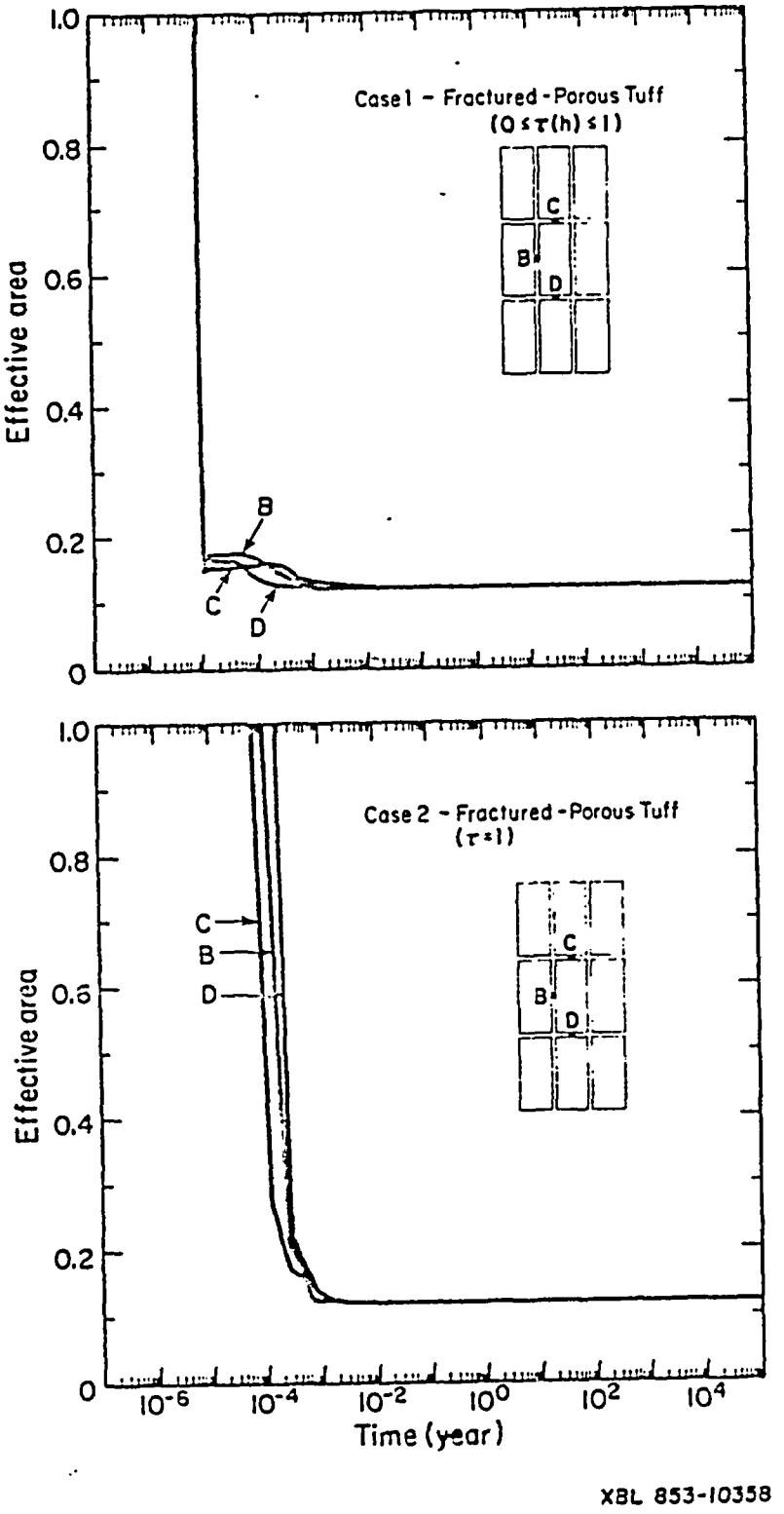

Figure 14. Effective fracture-matrix flow area changes at discrete points during drainage of a fractured tuff column.

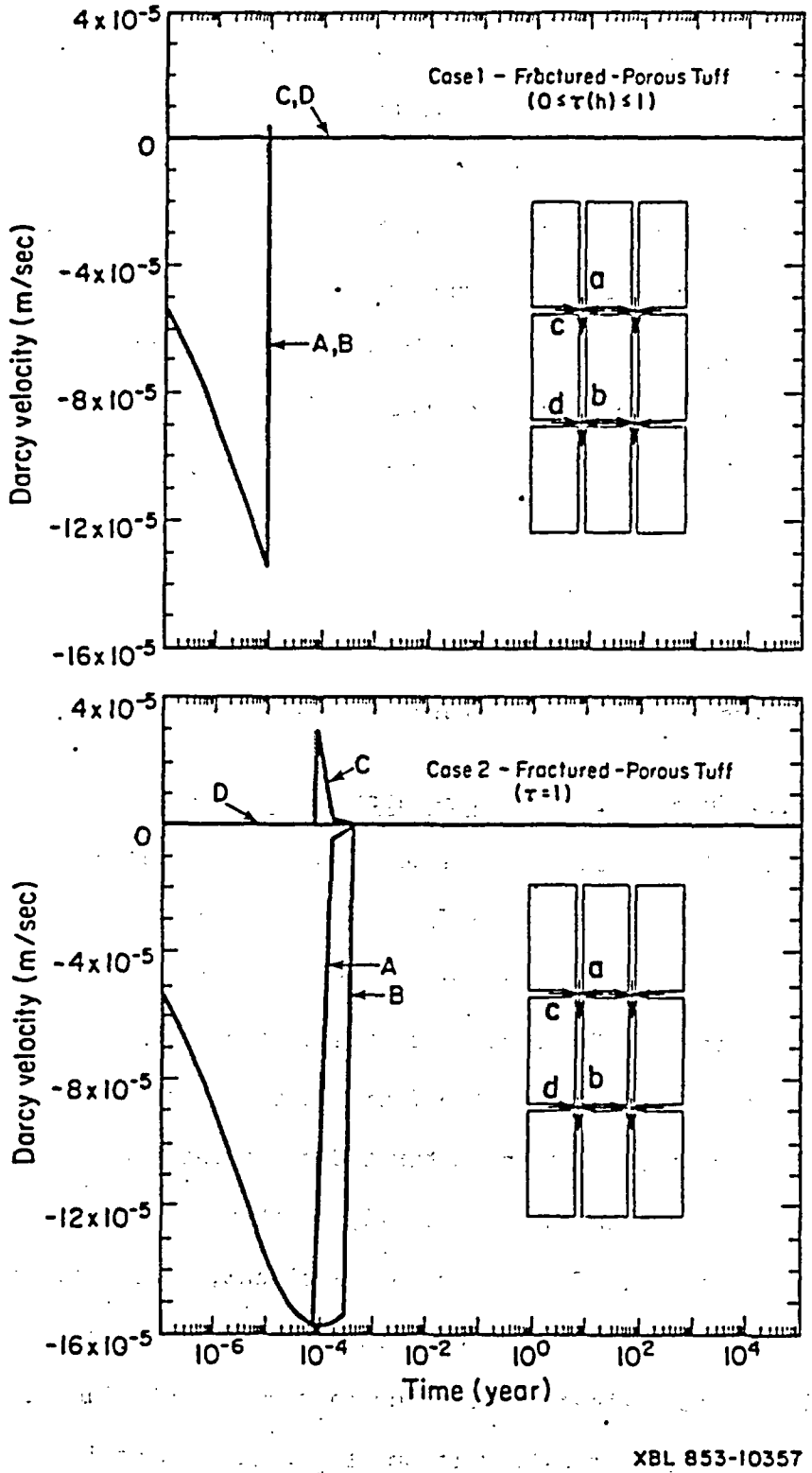

Figure 15. Darcy velocities along discrete fractures during drainage of a fractured tuff column. (sign convention for horizontal flow: positive - into the intersection, negative - away from the intersection; vertical flow: positive - upward, negative - downward).

velocity increases rapidly and peaks just before the fractures desaturate. After the transition to matrix flow, fluid velocities in fractures are essentially zero. The flows in the fracture at different locations are sensitive to the phase-separation constriction factor. In Case 2 with $\tau = 1$, the fluid moves more easily through the fractures before desaturation than in Case 1 with $0 \leq \tau(h) \leq 1$. The differences in velocities at different locations for Case 2 are more pronounced than for Case 1. The fluid in horizontal fractures moves towards the vertical fractures before they are drained. Just before vertical fracture flow stops, horizontal flow peaks. This is more evident in Case 2 than in Case 1. This again indicates that fracture flow in the transition from saturated to desaturated condition is sensitive to the details of fracture characteristics.

Darcy Velocity Changes in Fracture-Matrix Interfaces

Figure 16 illustrates the changes in Darcy velocities across the fracture-matrix interfaces at the mid-points of fractures. The fracture-matrix flow velocities are much smaller than the fracture-flow velocities in Figure 15. Before the fractures desaturate, the fluid in the matrix flows toward the fractures to supply the fluid in the fractures which is drained rapidly by the suction. At the saturated-desaturated transition, these matrix-fracture flows change drastically. After the transition, the fluid mainly moves vertically from upper matrix blocks, across horizontal fractures, and into lower matrix blocks. The horizontal flow also reverses direction from a initial matrix-to-fracture flow to a small but significant fracture-to-matrix flow. After the transition, the fractures no longer transmit fluid and become a small fluid storage source to feed the matrix blocks as they drain.

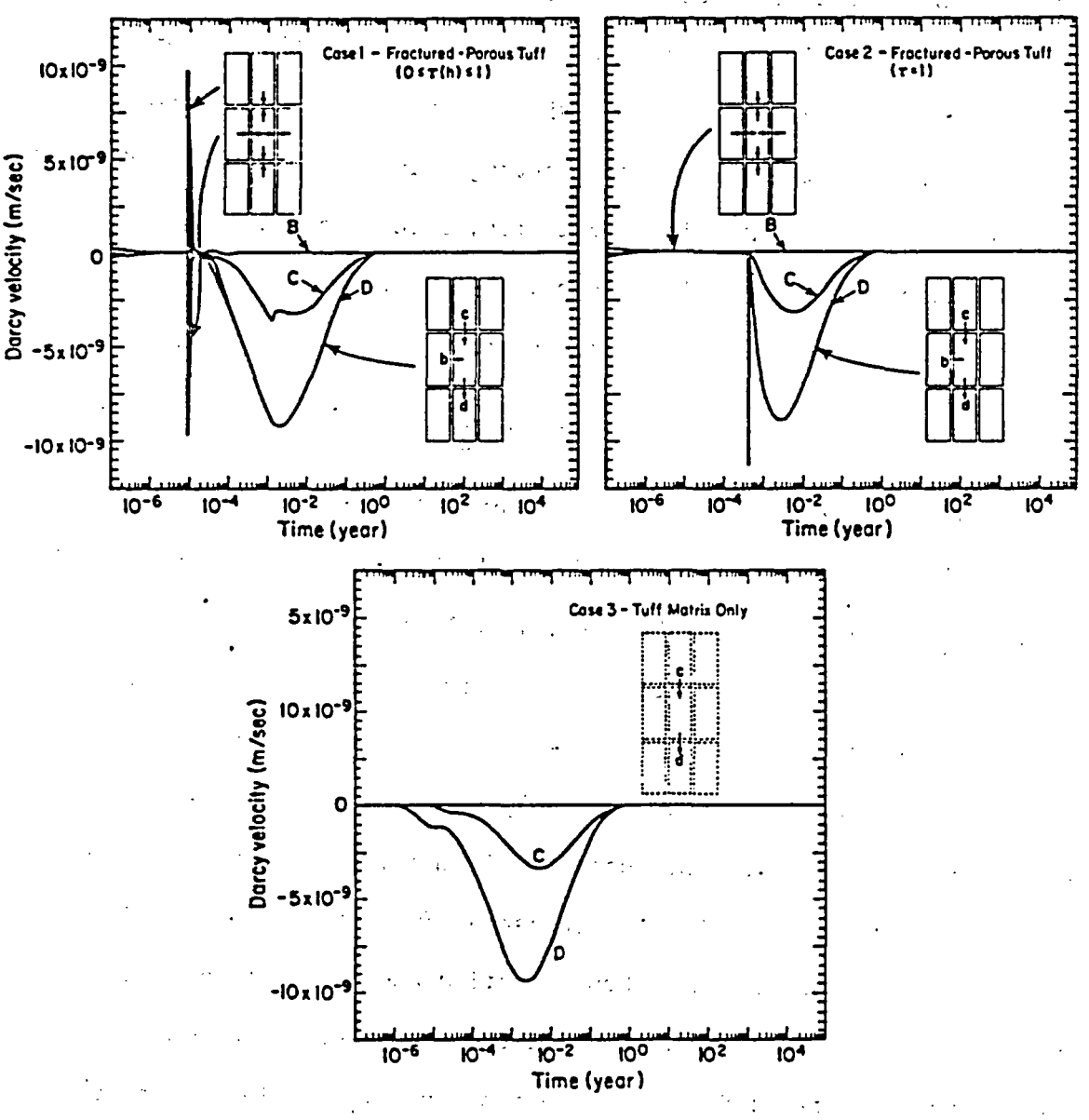

Figure 16. Darcy velocities at the fracture-matrix interfaces during drainage of a fractured tuff column (sign convention for horizontal flow: positive - matrix into fracture, negative - fracture into matrix; vertical flow: positive - upward, negative - downward).

After the fractures desaturate, the Darcy velocities from one matrix block across a fracture into the next matrix block are essentially the same as those calculated by a matrix-only model, as illustrated in Case 3, Figure 16 for a tuff-matrix column without fractures. The agreement among the velocities in Cases 1, 2, and 3 strongly indicates that the fluid-flow field of a partially saturated, fractured, porous formation can be simulated without taking fractures into account, if the transition region from saturated to unsaturated condition is not of concern.

SUMMARY

From the cases simulated for a fractured, porous tuff column with discrete fractures and porous blocks explicitly taken into account, the quasi-steady changes of the fluid-flow field of a partially saturated, fractured, porous system could be simulated approximately without taking fractures into account. However, the highly transient changes in flow from fully saturated conditions to partially saturated conditions are extremely sensitive to the fracture properties. On the one hand, the ambient, steady-state flow field of a partially saturated, fractured porous tuff system probably can be understood without detailed knowledge of the discrete fracture network properties. Under large suctions, the porous matrix is the main conduit for fluid flow. On the other hand, detailed information on fracture network geometry and discrete fracture characteristics is needed to fully understand the responses of a fractured-porous system to perturbations, such as an extreme flood event, which may cause transitions between partially saturated and fully saturated conditions.

Only one set of material properties has been simulated for the Topopah Spring Member. Not all of the required properties for simulations of the

fractured tuff are available. We have developed a statistical theory and have derived explicit formulae for the fracture characteristics based on well established capillarity theory and recent advances in rough fracture flow laws. The input data for the fracture properties, such as the spacing and the aperture distribution parameters, are derived from available fracture data. Some of the simplistic assumptions about fracture properties can be easily modified as more data become available. We expect that we will gain additional physical insight as we study more realistic simulations.

We believe that our basic conceptual model, based on an extension of soil physics of heterogeneous systems to a fractured, porous medium, is sound. Some of the detailed descriptions and assumptions, such as the reduction of the effective fracture-matrix flow area and the existence of a discontinuous liquid phase on the fracture surfaces, should become better established as experimental verification and more detailed numerical simulations are obtained. The tools needed for detailed numerical simulations are available. The logical task now is to closely couple these capabilities and modeling exercises with experimental investigations to better understand and assess the impact the hydrology of the partially saturated fractured, porous tuff formations on the performance of a repository.

REFERENCES

Boussinesq, J., 1868. Memoire sur l'influence des frottements dans les movements repuliers des fluides, J. Math. Pure Appl. Ser. 2, Vol. 13, pp. 377-424.

Carr, W. J. , 1974. Summary of tectonic and structural evidence for stress orientation at the Nevada Test Site, U.S. Geological Survey Report OFR-74-176, 53 p.

Duff, I. S., 1977. MA28 - A set of Fortran subroutines for sparse unsymmetric linear equations, Report AERE-R 8730, Harwell/Oxfordshire, Great Britain.

Evans, D. D., and C. H. Huang, 1982. Role of desaturation on transport through fractured rock, in "Role of the Unsaturated Zone in Radioactive and Hazardous Waste Disposal", pp. 165-178, edited by J. Mercer, P. S. Rao and I. W. Marine, Ann Arbor Science Publisher, Ann Arbor, MI.

Hayden, H., R. R. Peters, and J. K. Johnstone, 1983. Parameters and material properties for hydrologic modeling of the Topopah Spring Unit, memorandom to distribution, 9/27/83, Sandia National Laboratories, Albuquerque, NM.

Iwai, K., 1976. Fundamental Studies of Fluid Flow Through a Single Fracture, Ph.D. Thesis, Department of Civil Engineering, University of California, Berkeley, CA , 208 p.

Mualem, Y., 1976. A new model for predicting the hydrologic conductivity of unsaturated porous media, Water Resources Research, Vol. 12, pp. 513-522.

Narasimhan, T. N., P. A. Witherspoon, and A. L. Edwards, 1978. Numerical model for saturated-unsaturated flow in deformable porous media, Part 2, the algorithm, Water Resources Research, Vol 14, pp. 255-261.

Pickens, J. F., R. W. Gillham, and D. R. Cameron, 1979. Finite-element analysis of the transport of water as solute in tile-drained soils, J. Hydrology, Vol. 4, pp. 243-264.

Pruess, K., and T. N. Narasimhan, 1982. A practical method for modeling fluid and heat flow in fractured porous media, Paper SPE-10509, Proceedings of the Society of Petroleum Engineering Symposium on Reservoir Simulation, New Orleans, LA , pp. 269-284.

Scott, R. B., R. W. Spengler, S. Diehl, A. R. Lappin, and M. P. Chornack, 1982. Geologic character of tuffs in the unsaturated zone at Yucca Mountain, Southern Nevada, in "Role of the Unsaturated Zone in Radioactive and Hazardous Waste Disposal", pp. 289-335, edited by J. Mercer, P. S. Rao and I. W. Marine, Ann Arbor Science Publisher, Ann Arbor, MI.

Sinnock, S., Y. T. Lin, and J. P. Brannen, 1984. Preliminary bounds on the expected, postclosure performance of the Yucca Mountain repository site, Southern Nevada, Report SAND 84-1492, Sandia National Laboratories, Albuquerque, NM.

Spengler, R. W., and M. P. Chornack, 1984. Stratigraphic and structural characteristics of volcanic rocks in core hole USW-G4, Yucca Mountain, Nye County, Nevada, with a section of geophysical logs by D. C. Muller and J. E. Kibler, Report USGS-OFR-84-789, U. S. Geological Survey, Denver, CO.

Thordarson, W., 1983. Geohydrologic data and test results from well J-13, Nevada Test Site, Nye County, Nevada, Report Water Resources Investigations 83-4171, U.S. Geological Survey, Denver, CO.

Tsang, Y. W., and P. A. Witherspoon ,1981. Hydromechanical behavior of a deformable rock fracture, J. Geophysical Research, Vol. 86 (B10), pp. 9287-9298.

Tsang, Y. W., 1984. The effect of tortuosity on fluid flow through a single fracture, Water Resources Research, to be published.

Tyler, L. D., 1983. Minutes of June 23-24 Performance Assessment Working Group Meeting, memorandum to distribution, 7/29/83, Sandia National Laboratories, Albuquerque, NM.

van Genuchten, 1980. A closed-form equation for predicting the hydraulic conductivity of unsaturated soils, Soil Sci. Soc. Am. J., Vol. 44, pp. 892-898.

Winograd, I. J., and W. Thordarson, 1975. Hydrogeologic and hydrochemcial framework, South Central Great Basin, Nevada-California, with Special Reference to the Nevada Test Site, U. S. Geological Survey Professional Paper 712-C, pp. C1-126.

Witherspoon, P. A.,, J. S. Y. Wang, K. Iwai, and J. E. Gale, 1980, Validity of cubic low for fluid flow in a deformable rock fracture, Water Resources Research, Vol. 16, pp. 1016-1024.

DISTRIBUTION LIST

B. C. Rusche (RW-1)
Director
Office of Civilian Radioactive
Waste Management
U.S. Department of Energy
Forrestal Building
Washington, DC 20585

J. W. Bennett (RW-22)
Office of Geologic Repositories
U.S. Department of Energy
Forrestal Building
Washington, DC 20585

Ralph Stein (RW-23)
Office of Geologic Repositories
U.S. Department of Energy
Forrestal Building
Washington, DC 20585

J. J. Fiore, (RW-22)
Program Management Division
Office of Geologic Repositories
U.S. Department of Energy
Forrestal Building
Washington, DC 20585

H. W. Frei (RW-23)
Engineering & Licensing Division
Office of Geologic Repositories
U.S. Department of Energy
Forrestal Building
Washington, DC 20585

E. S. Burton (RW-25)
Siting Division
Office of Geologic Repositories
U.S. Department of Energy
Forrestal Building
Washington, D.C. 20585

C. R. Cooley (RW-24)
Geosciences & Technology Division
Office of Geologic Repositories
U.S. Department of Energy
Forrestal Building
Washington, DC 20585

T. P. Longo (RW-25)
Program Management Division
Office of Geologic Repositories
U.S. Department of Energy
Forrestal Building
Washington, DC 20585

Cy Klingsberg (RW-24)
Geosciences and Technology Division
Office of Geologic Repositories
U. S. Department of Energy
Forrestal Building
Washington, DC 20585

B. G. Gale (RW-25)
Siting Division
Office of Geologic Repositories
U.S. Department of Energy
Forrestal Building
Washington, D.C. 20585

R. J. Blaney (RW-22)
Program Management Division
Office of Geologic Repositories
U.S. Department of Energy
Forrestal Building
Washington, DC 20585

R. W. Gale (RW-40)
Office of Policy, Integration, and
Outreach
U.S. Department of Energy
Forrestal Building
Washington, D.C. 20585

J. E. Shaheen (RW-44)
Outreach Programs
Office of Policy, Integration and
Outreach
U.S. Department of Energy
Forrestal Building
Washington, DC 20585

J. O. Neff, Manager
Salt Repository Project Office
U.S. Department of Energy
505 King Avenue
Columbus, OH 43201

D. C. Newton (RW-23)
Engineering & Licensing Division
Office of Geologic Repositories
U.S. Department of Energy
Forrestal Building
Washington, DC 20585

O. L. Olson, Manager
Basalt Waste Isolation Project Office
U.S. Department of Energy
Richland Operations Office
Post Office Box 550
Richland, WA 99352

D. L. Vieth, Director (4)
Waste Management Project Office
U.S. Department of Energy
Post Office Box 14100
Las Vegas, NV 89114

D. F. Miller, Director
Office of Public Affairs
U.S. Department of Energy
Post Office Box 14100
Las Vegas, NV 89114

D. A. Nowack (12)
Office of Public Affairs
U.S. Department of Energy
Post Office Box 14100
Las Vegas, NV 89114

B. W. Church, Director
Health Physics Division
U.S. Department of Energy
Post Office Box 14100
Las Vegas, NV 89114

Chief, Repository Projects Branch
Division of Waste Management
U.S. Nuclear Regulatory Commission
Washington, D.C. 20555

Document Control Center
Division of Waste Management
U.S. Nuclear Regulatory Commission
Washington, D.C. 20555

S. A. Mann, Manager
Crystalline Rock Project Office
U.S. Department of Energy
9800 South Cass Avenue
Argonne, IL 60439

K. Street, Jr.
Lawrence Livermore National
Laboratory
Post Office Box 808
Mail Stop L-209
Livermore, CA 94550

L. D. Ramspott (3)
Technical Project Officer for NNWSI
Lawrence Livermore National
Laboratory
P.O. Box 808
Mail Stop L-204
Livermore, CA 94550

W. J. Purcell (RW-20)
Office of Geologic Repositories
U.S. Department of Energy
Forrestal Building
Washington, DC 20585

D. T. Oakley (4)
Technical Project Officer for NNWSI
Los Alamos National Laboratory
P.O. Box 1663
Mail Stop F-671
Los Alamos, NM 87545

W. W. Dudley, Jr. (3)
Technical Project Officer for NNWSI
U.S. Geological Survey
Post Office Box 25046
418 Federal Center
Denver, CO 80225

NTS Section Leader
Repository Project Branch
Division of Waste Management
U.S. Nuclear Regulatory Commission
Washington, D.C. 20555

V. M. Glanzman
U.S. Geological Survey
Post Office Box 25046
913 Federal Center
Denver, CO 80225

P. T. Prestholt
NRC Site Representative
1050 East Flamingo Road
Suite 319
Las Vegas, NV 89109

J. B. Wright
Technical Project Officer for NNWSI
Westinghouse Electric Corporation
Waste Technology Services Division
Nevada Operations
Post Office Box 708
Mail Stop 703
Mercury, NV 89023

M. E. Spaeth
Technical Project Officer for NNWSI
Science Applications
International, Corporation
2769 South Highland Drive
Las Vegas, NV 89109

ONWI Library
Battelle Columbus Laboratory
Office of Nuclear Waste Isolation
505 King Avenue
Columbus, OH 43201

SAIC-T&MSS Library (2)
Science Applications
International, Corporation
2950 South Highland Drive
Las Vegas, NV 89109

W. M. Hewitt, Program Manager
Roy F. Weston, Inc.
2301 Research Blvd., 3rd Floor
Rockville, MD 20850

W. S. Twenhofel, Consultant
Science Applications
International, Corp.
820 Estes Street
Lakewood, CO 80215

H. D. Cunningham
General Manager
Reynolds Electrical &
Engineering Co., Inc.
Post Office Box 14400
Mail Stop 555
Las Vegas, NV 89114

A. E. Gurrola
General Manager
Energy Support Division
Holmes & Narver, Inc.
Post Office Box 14340
Las Vegas, NV 89114

T. Hay, Executive Assistant
Office of the Governor
State of Nevada
Capitol Complex
Carson City, NV 89710

J. A. Cross, Manager
Las Vegas Branch
Fenix & Scisson, Inc.
Post Office Box 15408
Las Vegas, NV 89114

R. R. Loux, Jr., Director (3)
Nuclear Waste Project Office
State of Nevada
Capitol Complex
Carson City, NV 89710

N. E. Carter
Battelle Columbus Laboratory
Office of Nuclear Waste Isolation
505 King Avenue
Columbus, OH 43201

C. H. Johnson, Technical
Program Manager
Nuclear Waste Project Office
State of Nevada
Capitol Complex
Carson City, NV 89710

John Fordham
Desert Research Institute
Water Resources Center
Post Office Box 60220
Reno, NV 89506

Dr. Martin Mifflin
Desert Research Institute
Water Resources Center
Suite 1
2505 Chandler Avenue
Las Vegas, NV 89120

Department of Comprehensive Planning
Clark County
225 Bridger Avenue, 7th Floor
Las Vegas, NV 89155

Lincoln County Commission
Lincoln County
Post Office Box 90
Pioche, NV 89043

Community Planning and Development
City of North Las Vegas
Post Office Box 4086
North Las Vegas, NV 89030

City Manager
City of Henderson
Henderson, NV 89015

N. A. Norman
Project Manager
Bechtel National Inc.
P. O. Box 3965
San Francisco, CA 94119

T. N. Narasimhan (10)
Lawrence Berkeley Laboratory
1 Cyclotron Road
Berkeley, CA 94720

P. A. Witherspoon
Lawrence Berkeley Laboratory
1 Cyclotron Road
Berkeley, CA 94720

W. E. Wilson
U. S. Geological Survey
P.O. Box 25046
M.S. 416
Denver Federal Center
Denver, CO 80225

Planning Department
Nye County
Post Office Box 153
Tonopah, NV 89049

Economic Development Department
City of Las Vegas
400 East Stewart Avenue
Las Vegas, NV 89101

Director of Community Planning
City of Boulder City
Post Office Box 367
Boulder City, NV 89005

Commission of the European Communities
200 Rue de la Loi
B-1049 Brussels
BELGIUM

R. Harig
Parsons Brinckerhoff Quade & Douglas, Inc.
1625 Van Ness Ave.
San Francisco, CA 94109-3678

J. S. Y. Wang (10)
Lawrence Berkeley Laboratory
1 Cyclotron Road
Berkeley, CA 94720

Dr. T. R. Pigford
Department of Nuclear Engineering
University of California
Berkeley, CA 94720

B. J. Travis
Los Alamos National Laboratory
P.O. Box 1663
Los Alamos, NM 87545

6300 R. W. Lynch
6310 T. O. Hunter
6310 NNWSICF
6311 L. W. Scully
6311 L. Perrine (2)
6312 F. W. Bingham
6312 J. W. Braithwaite
6312 A. L. Dudley
6312 N. K. Hayden
6312 R. R. Peters
6312 M. S. Tierney
6313 T. E. Blejwas
6313 E. A. Klavetter
6313 R. M. Zimmerman
6314 J. R. Tillerson
6314 J. A. Fernandez
6314 A. J. Mansure
6315 S. Sinnock (5)
6315 Y. T. Lin
6315 T. S. Ortiz
6315 D. H. Zeuch
6332 WMT Library (20)
6430 N. R. Ortiz
3141 C. M. Ostrander (5)
3151 W. L. Garner (3)
8024 M. A. Pound
DOE/TIC (28)
(3154-3, C. H. Dalin)